Gravity and magnetic evidence for the geological setting of major mineral systems of the main metallogenic belts in South China: A qualitative analysis

Jiayong Yan[1,2], Qingtian Lü[1*,2], Fan Luo[1,2,3], Shaobo Cheng[1,2], Kun Zhang[1,2],Yongqian Zhang[1,2], Yao Xu[1,2],Chong Zhang[1,2],Zhendong Liu[1,2],Shuai Ruan[1,2], Xu Wang[1,2]

[1]*Chinese Academy of Geological Sciences, Beijing, 100037, China*

[2]*China Deep Exploration Center, China Geological Survey & Chinese Academy of Geological Sciences, Beijing, 100037, China*

[3]*School of Geophysics and Measurement-control Technology, East China University of Technology, Nanchang,330013, Jiangxi China*

Corresponding author: Qingtian Lü (lqt@cags.ac.cn)

Key Points:

- Vertical interface,tectonic framework,3D density and susceptibility model in South China were obtained by processing and inversion of gravity and magnetic data.
- The source zones and pathways of the mineral systems in major metallogenic belts in South China are revealed.
- Termination sites of main mineral systems in South China are uncovered by 3D Physical property model.

Abstract

South China(SC) is characterized by large-area multistage magmatism.There are five large-scale metallogenic belts in SC, multiple world-class deposits have been discovered, showing great prospecting potential. What led to the difference in the type and metal association of the deposits? What controls the distribution of the different types of metallogenic belts? Where can we find new deposits? To address these concerns, it is necessary to consider the metallogenic factors based on mineral system. Firstly,the satellite gravity was converted into Bouguer gravity under spherical coordinates. Then the reduction-to-the pole (RTP) magnetic anomalies in SC were obtained using the moving window with different geomagnetic parameter respectively.Further to that, inversion of gravity and magnetic data was applied to calculate the vertical lithospheric interfaces,and then the possible metallogenic source zones of the five metallogenic belts were analyzed. The distribution of main faults were determined and the boundaries among Yangtze Block (YB), Cathaysia Block (CB) and Jiangnan Orogenic belt (JNO) were redefined by multiscale edge detection of gravity and magnetic data,then the ore-forming pathways in the main metallogenic belts were explored. 3D spatial distribution of intrusions qualitatively identified by inverted susceptibility and density model , and hence the depositing site of Cu, Fe, Au, W and Sn deposits were inferred. The metallogenic source zones, pathways, and sites of the deposits of the mineral system in SC were qualitatively identified according to the gravity and magnetic data analysis , providing indications for future prospecting exploration in SC.

1 Introduction

A mineral system is defined as all geological factors that control the generation and preservation of mineral deposits (Wyborn et al., 1994; Zhai, 1999). These factors include the geological setting (including geodynamic and lithosphere architecture); the driver; timing and duration of mineralization; source of the fluid and mineralizing components; the pathways along which fluids (including magmas) flow; the depositional site and post-depositional modifications, which can be further classified as three basic components of “source”, “pathway”, and “site” (Huston et al., 2016; McCuaig et al., 2016; McCuaig and Hronsky, 2014). From initiation by deep

processes to the formation of a series of deposits, a mineral system will leave behind various physical, chemical, and mineralogical changes(just like footprints of metallogenic process) in the lithosphere. These “footprints” are detectable due to the petrophysical properties diffrences induced by altered,thus, geophysical exploration of mineral systems is more and more used in the study of metallogeny and target prediction (Lü et al., 2019). For example, Griffin et al. (2013) found that magma deposits of diamond and Ni-Cu (PGE) get their ore-forming components from the mantle lithosphere and mapping the structure of the lithosphere is needed for effective exploration. By a magnetotelluric (MT) and seismic reflection exploration, Heinson et al. (2018) have revealed the processes of formation from a deep-source region to mineral occurrences of the world-class IOCG Olympic Dam deposit.

The South China Block(SCB) is one of the most important polymetallic metallogenic provinces in the world. Large-scale mineralization occurred from the Proterozoic to Cenozoic, including Paleo-Mesoproterozoic IOCG, Neoproterozoic magmatic Cu-Ni sulfide and orogenic Au, Neoproterozoic-Early Paleozoic sedimentary Ni-Mo-PGE, P and Mn, Early Paleozoic granite related W-Mo, low-temperature Au-Sb, Indosinian MVT Pb-Zn-Ag, Carlin-type Au and vein-type Sb, and Early-Late Yanshannian porphyry-skarn W-Sn-Cu-Mo-Pb-Zn, low-temperature Au-Sb, etc. (Hu et al., 2017). There are five large-scale metallogenic belts only in the east of SC, namely the Middle-Lower Yangtze River Metallogenic Belt (MLYMB), Qingzhou-Hangzhou Metallogenic Belt (QHMB), Nanling Metallogenic Belt (NLMB), Wuyishan Metallogenic Belt (WYSMB), and Xiangxi-E’xi Metallogenic Belt (XEMB). Furthermore, multiple world-class deposits have been discovered in this area, showing excellent prospecting potential. The Mesozoic large granite province in SC and the mineral system related to granitoids are one of the most important metallogenic characteristics of SC, and it attracted the full attention of geologists. At present, the understanding of metallogenesis in SC has broken through the single magmatic-hydrothermal metallogenic model in the past, and many new metallogenic models have been established from the viewpoint of multi-stage, multi genesis and

multi-source(Hu and Zhou, 2012; Mao et al., 2013). However, the critical problems related to the mineral system, i.e., the source of metallogenic materials, deep process, and structural background of the mineral system, have not been clarified.

As we know, the regional gravity and magnetic field contain abundant information about underground structure and material composition(Guo and Gao,2018). Therefore, the processing and inversion of such information make it practicable to discuss the critical metallogenic factors of a mineral system from three aspects: vertical layers, horizontal boundaries, and 3D morphology of key geological bodies such as intrusion. In this paper, the satellite gravity was first converted into Bouguer gravity based on spherical coordinates. Then the reduction-to-the pole (RTP) satellite magnetic anomalies in SC were obtained using the moving window method of RTP. Further to that, inversion of gravity and magnetic data was applied to calculate the vertical lithospheric interfaces of Moho depths, isostatic gravity anomalies, and mantle gravity anomalies as well as magnetic basement in SC. Based on this, the possible metallogenic source zones and background of the five metallogenic belts were analyzed. Multiscale edge detection for potential field data was also applied in this paper. As a result, the distribution of main faults in SC was determined, the boundaries of Yangtze Block (YB), Cathaysia Block (CB), and Jiangnan Orogenic belt (JNO) were redefined, and the ore-forming pathways or pathway footprints in the main metallogenic belts were explored. 3D density and susceptibility model of SC was obtained by 3D gravity and magnetic physical properties inversion. Based on the models, it was considered that the 3D spatial distribution of intrusions could be qualitatively reflected by the associations of high-susceptibility bodies and low-density bodies, and hence the depositing position of Cu, Fe, Au, W, and Sn deposits were inferred. In summary, the metallogenic source zones, pathways, and sites of the deposits in SC were qualitatively identified according to the gravity and magnetic field analysis of the mineral systems in this area.

2 Geological setting

The SCB is one of the major blocks that constitute the Chinese mainland. The Qinling-Dabie orogen bounds it from the North China Craton in the north, Longmenshan Fault from the Songpan-Gantze terrane in the northwest, Ailaoshan-Songma suture zone from Indochina Block in the southwest and the Pacific Ocean to the southeast (Figure1). The SCB consists of the YB in the northwest and the CB in the southeast, which were welded along the Jiangnan belt during Neoproterozoic (Cawood et al., 2020).

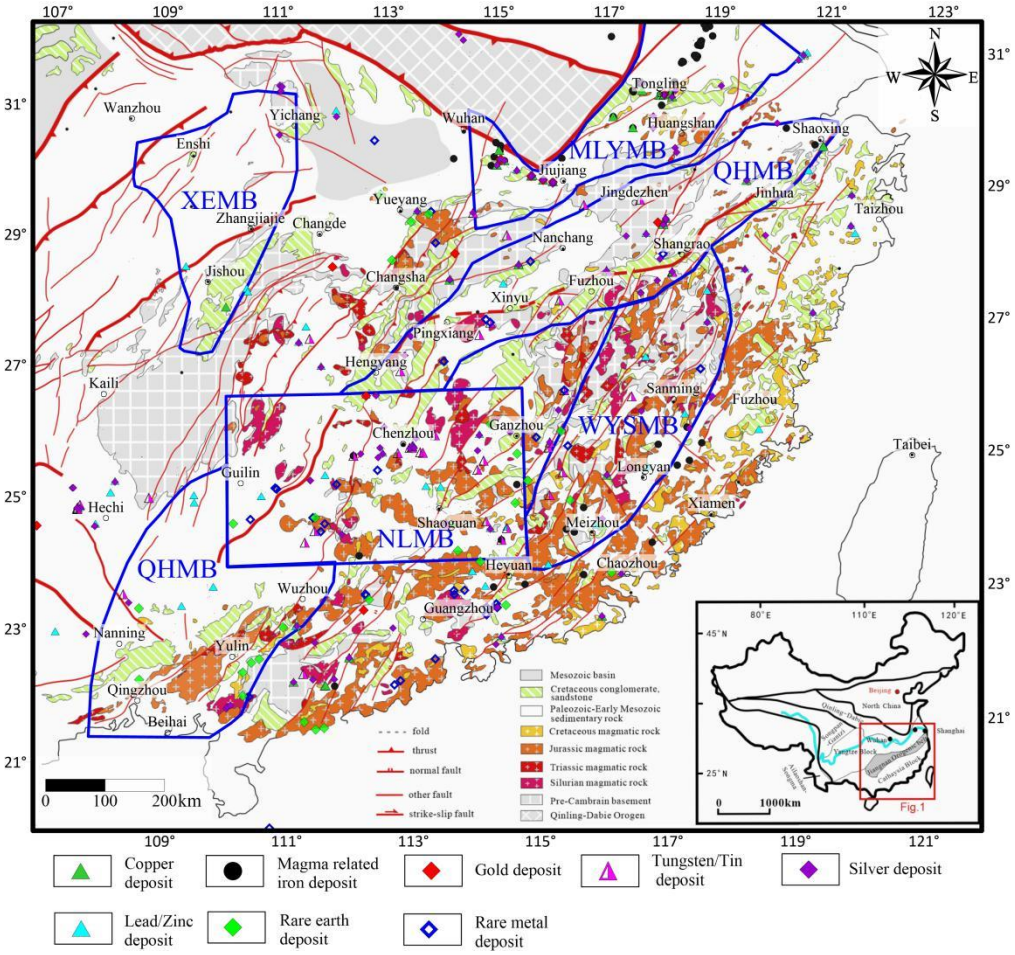

Figure1. Geological setting and mineral deposit distribution of South China (blue polygons are outline of 5 metallogenic belts,MLYMB: Middle-Lower Yangtze River Metallogenic Belt, QHMB: Qingzhou-Hangzhou Metallogenic Belt, WYSMB: Wuyishan Metallogenic Belt, NLMB: Nanling Metallogenic Belt, XEMB: Xiangxi-E'xi Metallogenic Belt)

In YB, the Precambrian basement is mainly made up of Proterozoic lithologies,

with minor exposed Archean rocks. The rare Archean-Paleoproterozoic rocks consist of Kongling Complex, Huangtuling granulites, Yudongzi Group and Houhe Complex from the northern, and Dahongshan and Dongchuan groups from the southwestern part of the block (Chen et al., 2019; Greentree and Li, 2008; Li et al., 2014; Liu et al., 2019; Wang and Zhou, 2014; Wu et al., 2008; Zhao et al., 2010). These crystalline basements are surrounded by Late Mesoproterozoic to Middle Neoproterozoic strata (e.g., Huili Group, Sibao Group, and equivalent sequences) along the Panxi-Hannan Belt and Jiangnan Orogen which are locally unconformably overlain by Nanhua (e.g., Banxi Group) and Sinian systems (equivalent to Cryogenian and Ediacaran) (Wang et al., 2012; Zhao and Cawood, 2012). Neoproterozoic magmatic rocks are widespread along the Jiangnan Orogen and margins of the YB (Xia et al., 2018; Zhao et al., 2018a; Zhu et al., 2019). The sedimentary cover of YB consists mainly of Cambrian to Triassic marine sedimentary rocks and Jurassic-Cretaceous and Cenozoic continental sedimentary rocks.

In CB, no exposed Archean rocks have been reported, and the oldest rocks are Paleoproterozoic granitoids and supracrustal rocks which distribute in the Wuyishan area, the northeastern part of the block (Liu et al., 2014; Yu et al., 2012; Zhao et al., 2018b). Minor Mesoproterozoic basement rocks only occur on Hainan island and consist of Baoban Group, Shilu Group, and Shihuiding Formation (Yao et al., 2019; Zhang et al., 2019). Neoproterozoic lithologies are the dominated Precambrian basement in the CB, including Chencai, Longquan, Mayuan, Mamianshan, Wanquan, Shenshan, and Yunkai Groups, spreading along Chencai-Wuyishan-Nanling-Yunkai area (Charvet, 2013; Shu et al., 2011; Yang and Jiang, 2019; Yu et al., 2010). Different from the YB, Late Ordovician to Middle Devonian strata are absent in the CB, and it is featured by numerous Phanerozoic igneous rocks, especially Mesozoic granitoids.

The SCB has witnessed a prolonged and complicated evolution. Revealed by geochronology and geochemistry data from the Kongling Complex, the continental nucleus of YB probably grown in Archean (Li et al., 2014; Li et al., 2018; Qiu et al., 2018). The 2.1-1.8 Ga magmatic and metamorphic events and ~1.7-1.5 Ga continental

rifting magmatism suggest that the YB has probably been involved in the assembly and breakup of Columbia (Han et al., 2017; Yin et al., 2013; Zhang et al., 2012). Although there have no exposed Archean rocks in the Cathaysia, Archean detrital and inherited zircons imply that it is either underlain by Archean crust or developed on the margin of an Archean block (Wang et al., 2020; Xu et al., 2016; Zhao and Cawood, 2012). During Neoproterozoic, the Yangtze and Cathaysia collided along the Jiangnan Orogen to form the unified SCB, which is later than the typical Grenvillian orogenesis marking the assembly of the supercontinent Rodinia (Wang et al., 2019; Yao et al., 2019; Zhao, 2015). Then the early Paleozoic intracontinental orogeny created deformation, ductile shearing, and angular unconformities between the Sinian to lower Paleozoic strata and is responsible for voluminous granitic rocks in the CB (Charvet, 2013; Yan et al., 2017; Zhang et al., 2017). During Mesozoic, the SCB collided with the North China Craton in the Triassic (Wu and Zheng, 2013). In response to the subduction of the Paleo-Pacific Plate, numerous magmatism emplaced in the whole CB and southeastern YB, which is well known as the SC large granitic province (Li et al., 2019). With these tectonic-igneous activities, multiple metallogenic events occurred, and several metallogenic belts formed in the SCB (Hu et al., 2017). Here we focus on some of the significant metallogenic belts, and the brief descriptions are as following:

The V-shaped MLYMB along the northern margin of the YB is bounded by the Xiangfan-Guangji Fault in the northwest, the Tancheng-Lujiang Fault in the northeast and the Yangxing-Changzhou Fault in the south. The MYLB is characterized by Yanshannian Cu-Fe polymetallic mineralization, which mainly occurs in seven ore concentration areas, including Edongnan, Jiurui, Anqing-Qiuchi, Luzong, Tongling, Ningwu, and Ningzhen. Among these clusters, Luzong and Ningwu are in the volcanic rift basins while the rest are in secondary uplifts. Two main types of ore deposits have been recognized in the belt: (1) 146~135Ma porphyry-skarn-strata bound Cu-Au-Mo-Fe deposits which are related to high-K calc-alkaline granitoids; (2) 135~126Ma magnetite-apatite deposits which are associated with shoshonitic rocks

(Mao et al., 2011; Zhou et al., 2015). The former mainly occurred in secondary uplifts and controlled by W-NW and E-W faults, while the latter distributes in rift basins and controlled by NE-NNE faults (Zhai et al., 1996).

The NMLB is located in the central part of the SCB, which covers south Jiangxi, south Hunan, north Guangxi and north Guangdong provinces (Chen et al., 2013; Li et al., 2018). The NLMB is famous for its tungsten and tin resources which account more than 70% W and 50% Sn reserves of China with several world-class deposits of Shizhuyuan W-Sn-Mo-Bi, Xihuashan W, Yaogagnxian W-Mo and Taoxikeng Pb-Zn-W-Mo, etc. (Li et al., 2020; Wang et al., 2007). The quartz-vein, skarn, and stratiform sulfide types are the main types of the deposits in the belt; other types include greisen, pegmatite, and volcanic types, etc. Besides the Caledonian granite-related W-Sn-Mo deposits such as Niutangjie, Yangjiaping and Yangjiashan, most of the deposits formed between 160 Ma and 150 Ma, genetically related to the coeval highly fractionated granitoid (Chen et al., 2018; Hu et al., 2012; Shu et al., 2011; Zhao et al., 2017). However, younger ages of 160-130Ma have also been obtained, indicating later mineralization events or hydrothermal metal redistribution (Legros et al., 2020; Wang et al., 2017).

The NNE trending QHMB extends along the Jiangshan-Shaoxing fault to the southeast from Qinzhou Bay in Guangxi, eastern Hunan, central Jiangxi to Hangzhou Bay in Zhejiang province. It locates in the southeastern margin of the Yangzte Block and tectonically belongs to the Jiangnan Orogen, which formed by the amalgamation of Yangzte and Cathyasia Blocks (Yang and Mei, 1997; Zhou et 2017). The QHMB is a famous Mesozoic Cu-Au polymetallic metallogenic belt with most of the deposits related to volcanic and granitoid (Ni and Wang, 2017). Mineralization mainly occurred in Jurassic (170-155Ma), representative deposits include Dexing porphyry Cu-Au-Mo, Yinshan epithermal Cu-Ag-Pb-Zn, Linhou hydrothermal vein Cu, Baoshan skarn Cu-Pb-Zn, and Yuanzhuding porphyry Cu-Mo, etc. (Mao et al., 2011; Mao et al., 2018; Tang et al., 2017). Recently, several porphyry-skarn W-Sn deposits, including world-class Zhuxi and Dahutang, have been discovered in the northern

Jiangxi and Anhui provinces (Huang and Jiang, 2014; Pan et al., 2017). These latest Jurassic to earliest Cretaceous deposits has defined a new tungsten belt, namely North Yangtze Tungsten Belt or Jiangnan Porphyry-skarn Tungsten Belt (Feng et al., 2018; Mao et al., 2017).

The NE trending WYSMB mainly covers southwestern Zhejiang, Fujian, and northeastern Guangdong provinces. It is located to the east of Nanling metallogenic Belt and separated from the Qinzhou-Hangzhou metallogenic Belt by the Jiangshan-Shaoxing fault to the north. Basement in the belt is made up of minor Paleoproterozoic and dominant Neoproterozoic metamorphic rocks. The phanerozoic cover consists of Early Paleozoic marine metasedimentary rocks, Devonian to Middle Triassic weakly metamorphic marine sedimentary rocks and Late Triassic to Cenozoic continental sedimentary rocks (Ding et al., 2016). The WYSMB is characterized by Yanshannian Cu-Zn-Pb polymetallic mineralization, which is represented by the Lengshuikeng porphyry Ag-Pb-Zn deposit in the northern part and the Zijinshan epithermal Cu-Au deposit in the southern part of the belt (Jiang et al., 2017; Qi et al., 2020).

Tectonically, the XEMB stretches over the northern margin of YB, Xuefeng Mountain, and the Jiangnan Orogen. It includes central-western Hunan and western Hubei provinces and contains great resources of Mn, Pb, Zn, and Sb. The sedimentary Mn deposits are mostly hosted in black shales of Nanhua Group and related to the formation of the Nanhua rifting basin during Late Neoproterozoic (Tang and Liu, 1999; Wu et al., 2016). The Caledonian Pb-Zn mineralization represented by the Huayuan deposit is hosted in the Sinian to Early Paleozoic carbonate rocks and are comparable to the MVT deposits in eastern Guizhou province (Li et al., 2014; Zhou et al., 2017). The XEMB preserves the largest Sb resource in the world, with most of Sb bearing veins occurring in the Proterozoic Lengjiaxi and Banxi Groups. Three major mineralization stages of Ordovician-Devonian, Late Triassic, and Later Jurassic-Early Cretaceous have been revealed by geochronology, and representative deposits include Woxi W-Sb-Au, Banxi, and Xikuangshan Sb deposits (Gu et al., 2012; Li et al., 2019;

Zhang et al., 2019).

3 The lithospheric architecture of South China inferred by gravity and magnetic dataset

3.1 Gravity and magnetic dataset

Currently, the ground gravity data has not covered the whole Chinese mainland since it is hard to conduct land gravity surveys in areas such as offshore and high-altitude areas, making it impossible to provide complete data for large-scale research. In contrast, satellite gravity data covers a wide area, and the data can be acquired conveniently despite its lower accuracy. They are furthermore less affected by near-surface density changes, which are associated with intracrustal geological features. A growing number of geophysicists are using satellite gravity data to study the distribution of subsurface structures over large mesoscale areas (ie.g. Tibet, North China Craton, Antarctic continent, Asia, et al.) (Li et al., 2020; Zhao et al., 2020; Pappa, 2020; Haeger et al., 2019; Steffen et al., 2017; Kaban et al., 2016).

The earth gravity field Model EIGEN6C4 data is composed of EGM2008 (Pavlis et al., 2012) (continent) and DTU global gravity anomaly grid (Ocean) (Ander et al., 2010). Eyike et al. (2010) is evaluated by comparison to ground gravity and EGM2008 gravity through upward continuation, spectral analysis and statistical evaluation. It is show that a strong similarity between EGM2008 and ground data can be confirmed. Interpretation of the EGM2008 data allows identifying and confirming the position of major structural trends and provides new information on the crustal architecture. Then the experimental results show that the accuracy of the satellite gravity data (EIGEN6C4) in SC is equivalent that of the ground gravity data with 5 km $\times$ 5 km (Huang et al., 2016). Therefore, the gravity data generated by the high-order gravity field model EIGEN-6C4 were used for deep structure explore in the east of SC. Because the research area is more than 1,600 km long from east to west and more than 1,300 km wide from north to south. The gravity anomalies in such a large area should be calculated based on spherical coordinates. We based on spherical coordinate to calculate the Bouguer gravity anomalies (Figure 2) in the east of SC (Luo et al., 2019; Uieda et al., 2015).

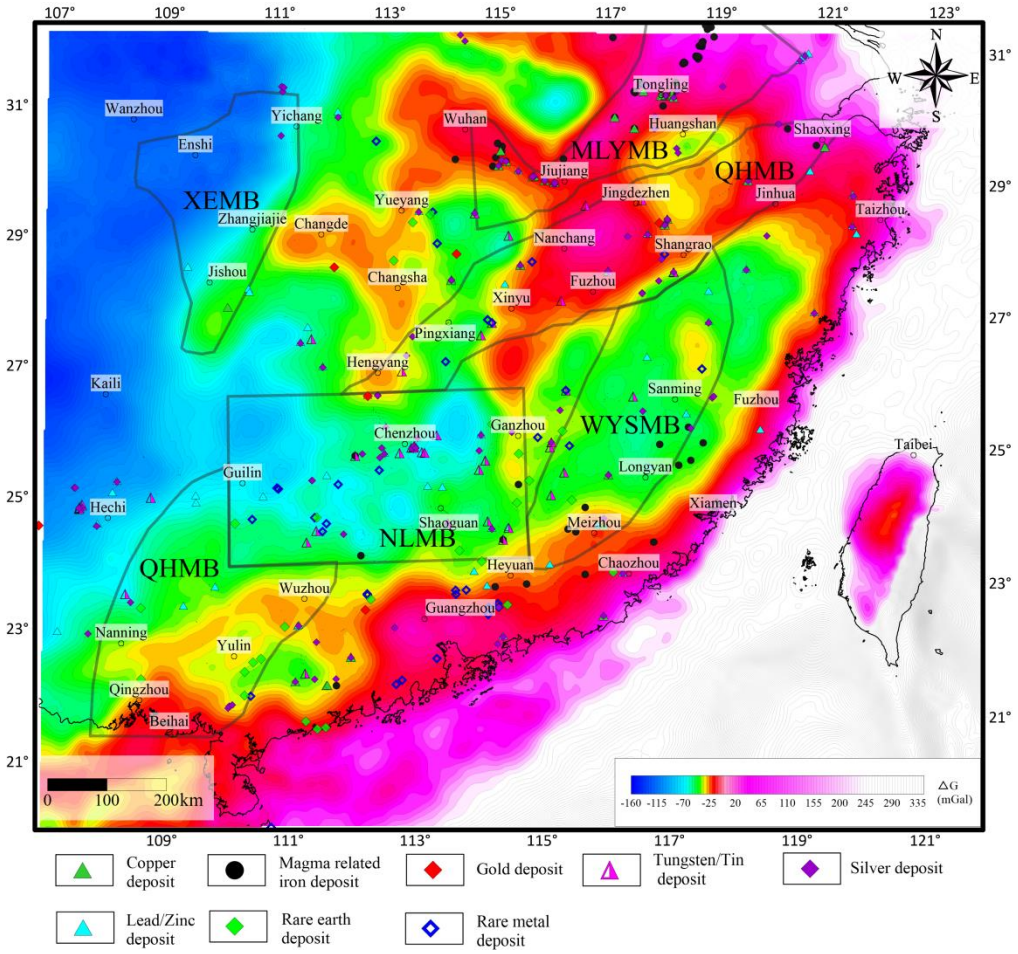

Figure 2. Bouguer gravity anomalies of South China calculated form satellite gravity data under spherical coordinates

Magnetic anomalies can be used to understand the subsurface structure and crustal composition deeply. The global Earth Magnetic Anomaly Grid EMAG2 was compiled based on satellite, ship, and airborne magnetic measurements.The EMAG2 data represents magnetic anomalies at 4 km altitude above the geoid in 2–arcmin resolution (Maus S et al., 2009). Li et al (2017) to obtain the global model of Curie-point depth based on EMAG2. Jaroslav et al. (2020) used the EMAG2 data to assist in the detection of subsurface structures on Greenland.

Since the magnetic field of the Earth is a dipole field, the center of induced magnetic anomalies tends to differ from the location of magnetic bodies. It is inclined towards the north in the Northern Hemisphere and towards the south in the Southern Hemisphere and varies with the latitudes. Therefore, this greatly disrupts the identification of magnetic anomaly boundaries and the projection of magnetic body positions onto a plane. For this reason, RTP is generally used to locate the center of

anomalies right above the magnetic body. It requires the geomagnetic parameters such as magnetic inclination and magnetic declination as the input. However, these parameters vary with longitudes, latitudes, and time. Using the parameters of the center of a magnetic body to conduct RTP is practicable for a relatively small area but impracticable for a large area since the parameters vary greatly in a large area (Guo et al. 2013). To reduce the influence of the change in magnetic parameters on RTP, the moving window method of RTP was adopted in this paper. The research area was divided into the windows of 300 km×300 km according to the experimental comparison. After RTP was conducted for all windows using different geomagnetic parameters, the windows were sutured together again. In this way, the EMAG2 of RTP magnetic anomalies (Figure 3) of SC was obtained.

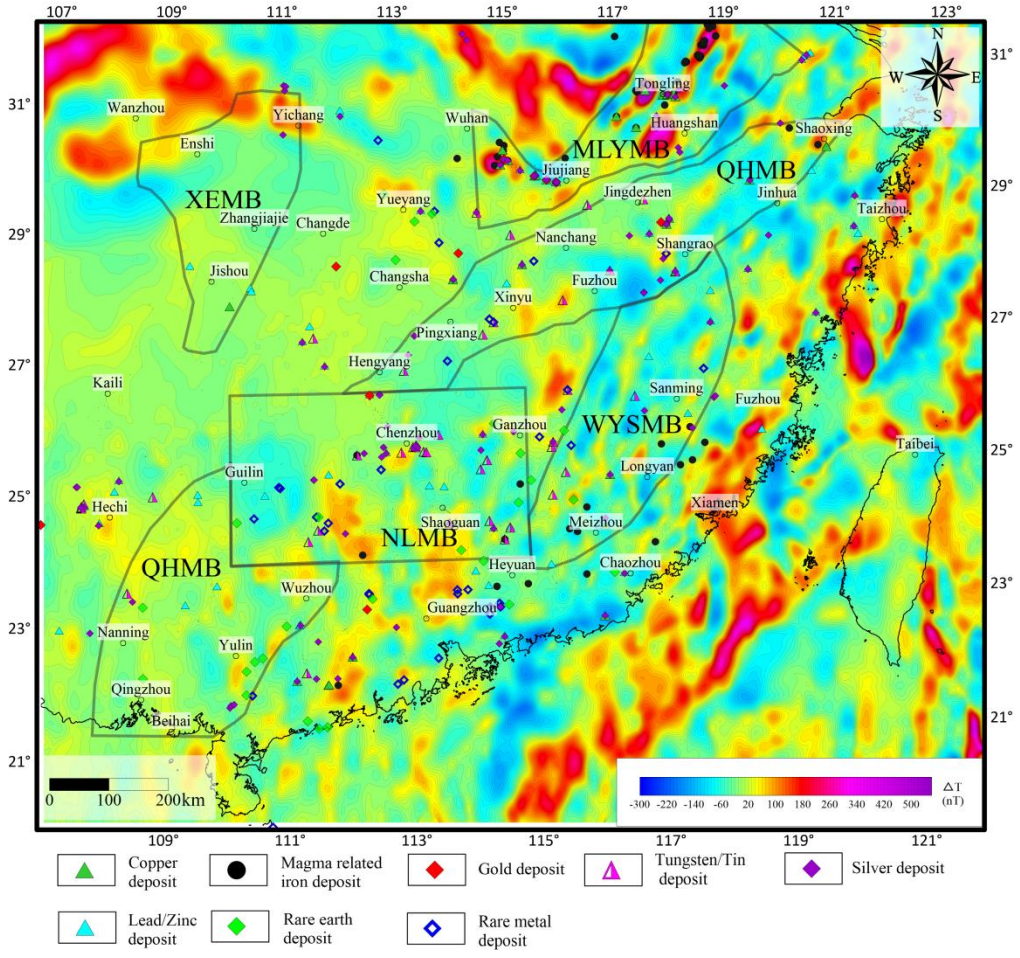

Figure 3. RTP magnetic anomalies of South China based on EMAG2

3.2 Moho depths variation

Mohorovicic discontinuity (Moho) is the boundary that lies between the lower

crust and the upper mantle of the Earth. It also serves as the dynamic boundary through which the crust and the mantle exchange their materials and energy, and thus controls the source zones of mineral systems. An effective means to determine the Moho depth variation is the density contrast interface inversion of gravity data since the gravity data feature a wide coverage and high-density sampling points compared with seismic or MT methods. Geophysicists have proposed a series of inversion methods after extensive research, including commonly used one and two-stage iterative method based on an approximate formula (Bott, 1960; Cordell and Henderson, 1968), the method of the compressed mass plane (Liu and Wang, 1977), the sinx/x method (Tomada and Aki, 1955; Tsuboi, 1956), and the spectral expansion method (Chavez and Garland, 1985). Most especially, the Parker-Oldenburg iterative inversion method in the frequency domain has been widely adopted owing to its fast calculation (Oldenburg, 1974; Parker, 1972). The density contrast and starting depth for flat interface are essential parameters in the density contrast interface inversion, and their values directly affect the accuracy of the inversion results. However, in the case where the traditional Parker-Oldenburg method is used to calculate density contrast interfaces, only a constant crust-mantle density contrast and a basic depth are used in the whole research area, without considering the transverse variation of Moho density contrast. This will result in errors when calculating the density interfaces of a large area. To overcome the shortcomings arising from constant density, a method of variable density was adopted in this paper. With this method, the research area was divided into regular rectangles that can be spliced together. After the determination of the crust-mantle density contrast for each rectangle reference the global crust model Crust1.0 density contrast information, Parker-Oldenburg iterative inversion was employed for each rectangle (Luo et al., 2019). In detail, the iterative inversion calculation was carried out with an improved Parker-Oldenburg formula (Luo et al., 2019), with the Bouguer gravity anomalies corrected for the sediment effect (Figure 2) and the variable Moho density contrasts in the Crust1.0 being used as the input data, the average crust thickness Z_0 being taken as 32 km, and the Moho depth variation (h) initially being taken as 0 km. In this way, the Moho depth variation in SC was achieved (Figure 4). The Moho depth in the middle and lower reaches of the Yangtze River is a case study to verify this method. It was revealed to be 29–35 km by Lü et al. (2015) through the results of several deep seismic reflection profiles arranged in the middle and lower reaches of the Yangtze River and was determined to 28–36 km by Shi et al. (2013) through the grid-search method of the

broadband seismic survey. In this paper, it was calculated to be 31–34 km by variable density contrast interface inversion of satellite gravity data, which coincides with the previous results based on the seismic survey. This indicates that the Moho depth determined by variable density contrast interface inversion of satellite gravity data is reliable.

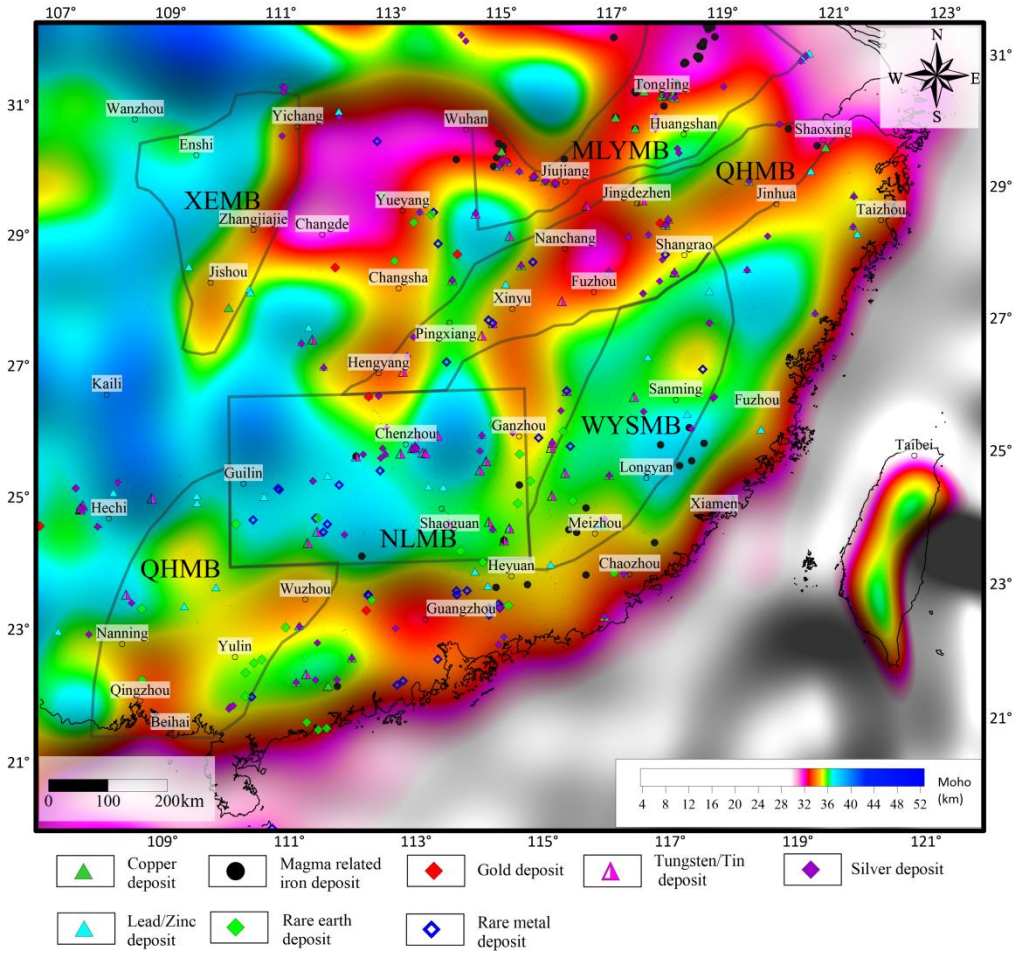

Figure 4. Moho depths in South China inverted by Park-Oldenburg iterative inversion method based on variable density contrast between crust and mantle constrained by Crust1.0

The Moho in SC tends to gradually deepen from east to west and from north to south in general, and varies greatly in local areas, with multiple intermittent mantle uplift areas and mantle subsidence areas existing. Xiangfan-Yichang-Zhangjiajie-Tongren-Liuzhou-Nanning area features noticeable Moho variation. It is part of Daxing'anling-Taihangshan-Xuefengshan gravity gradient belt in China that extends into SC. It is also the eastern longitudinal strip in "three latitudinal strips and two longitudinal strips" (the former refers to

Tianshan-Yinshan-Yanshan, Qinling-Dabie, and Nanling, and the latter refers to Daxing'anling-Taihangshan-Wulingshan, and Helanshan-Longmenshan), which is the geotectonic framework of China as proposed by Liu (2007). In JNO, the Moho depth ranges from 36–30 km, displaying certain features of being deep in the north and shallow in the south. The Moho gradually rises towards the hinterlands of the East China Sea and the South China Sea in the coastal areas of the SCB. The shallowest part is in the eastern and southern part of the Taiwan Island, with a depth of about 10 km, while it is the deepest on the northwestern margin of the SCB, with a depth of about 50 km. The high-value area in the southeast corner as shown in Figure 4 is the continental area of Taiwan Province, China, where the Moho depth ranges from 30–40 km. Besides, the MLYMB and QHMB are located in the Moho uplifts, NLMB and WYSMB in the Moho subsidence areas, and XEMB in the transitional zone between the Moho uplift and depression.

3.3 Mantle gravity anomaly

As shown by extensive research, the fluids that are widely distributed in the mantle serve as the medium and carrier for the migration of deep-source metallogenic materials and thus provide metallogenic materials and thermal source for the formation of large-super large deposits or ore concentration areas (Spera, 1987; Schneider and Eggler, 1986; Bolfan-Casanova, 2005; Mao et al., 2005). Not only do they affect the partial melting of mantle rocks and the properties of mantle-derived magma but also cause the heterogeneity of lithospheric mantle, thus leading to the formation of the transition between the depleted mantle and enriched mantle (Yang et al., 2008; Rickard and Roland, 2011). The mantle Bouguer gravity anomalies can be used to reflect the thickness of the crust and the density variation of the crust and the upper mantle, and can further reveal the mantle state. Therefore, they can be used to explore the deep mantle origin of research targets (Grindlay et al., 1998; Radhakrishna et al., 2008; Suo et al., 2016).

According to the division theory of the spherical structure of the Earth and the definition of gravity anomaly, the mantle Bouguer gravity anomalies (MBGA) are usually obtained by correcting free-air gravity anomalies for the effects caused by terrain, sediments, and crustal thickness (Prince and Forsyth, 1988; Suo et al., 2016; Deng et al., 2014; Mooney and Kaban, 2010). In this paper, the MBGA in SC were

383 determined as follows. First, based on the aforementioned crustal thickness in SC
384 (Figure 4) and the density data of transversely distributed blocky rectangles in Crust1.0
385 (Laske et al., 2012), forward calculation of transverse variable density was conducted
386 by the method proposed by Parker (1973) to determine the gravity response resulting
387 from the crustal thickness in the research area. Then the free-sediment effect Bouguer
388 gravity anomalies (Figure 2) minus the crust thickness gravity response value to
389 obtained the MBGA in SC (Figure 5). It is generally believed that the areas with high
390 MBGA reflect the thinning of the crust or the presence of high-density anomaly zones
391 in the crust/upper mantle, while the areas with low MBGA reflect the thickening of the
392 crust or the presence of low-density anomaly zones in the crust/upper mantle formed
393 owing to high temperature or partial melting (Corimer et al., 1995). Based on this, as
394 well as the Moho depths, as shown in Figure 4, it is believed that the areas with low
395 MBGA in the continental areas of the SCB such as MLYMB and QHMB mainly reflect
396 the thinning of the crust, while the areas with low mantle gravity anomalies such as
397 NLMB and WYSMB reveal the thickening of the crust and the presence of molten
398 low-density bodies in the upper mantle of these areas.

399 *3.4 Isostatic gravity anomaly*

400 Crustal isostasy is a hypothesis based on the principle of hydrostatic equilibrium.
401 According to this theory, the Earth's crust is composed of many rocks with different
402 thicknesses, which are floating in denser and plastic underlying magma and are in an
403 equilibrium state according to Archimedes' principle. This means that both the excess
404 of mass above sea level in continental and mountainous areas and the deficit in mass
405 below sea level in marine areas are to be compensated by denser magma (i.e.,
406 subsidence in continental areas and uplift in marine areas). That is, the increase or
407 decrease in mass in large areas on the ground is inevitable to be compensated
408 underground. As indicated by some geophysical and geodetic phenomena, isostatic
409 compensation covers about 90% of the Earth (Heiskanen et al., 1967). Therefore, it is
410 necessary to calculate the isostatic gravity anomalies in the process of in-deep Earth
411 research to reflect the real condition of the crustal structure correctly. The values of
412 isostatic gravity anomalies can be used to decide whether the deep crust is in an
413 equilibrium state. In a case where the crust is in a complete equilibrium state, the
414 isostatic gravity anomalies should be close to zero. Otherwise, the isostatic gravity
415 anomalies on the ground will be highly positive or negative. Positive anomalies

indicate excess compensation (i.e., in mantle uplift areas), while negative anomalies indicate deficit compensation (i.e., in mantle subsidence areas). A non-equilibrium state will inevitably lead to the occurrence of isostatic adjustments. Therefore, the research on isostatic gravity anomalies will contribute to the understanding of the characteristics of the tectonic activities in the deep crust.

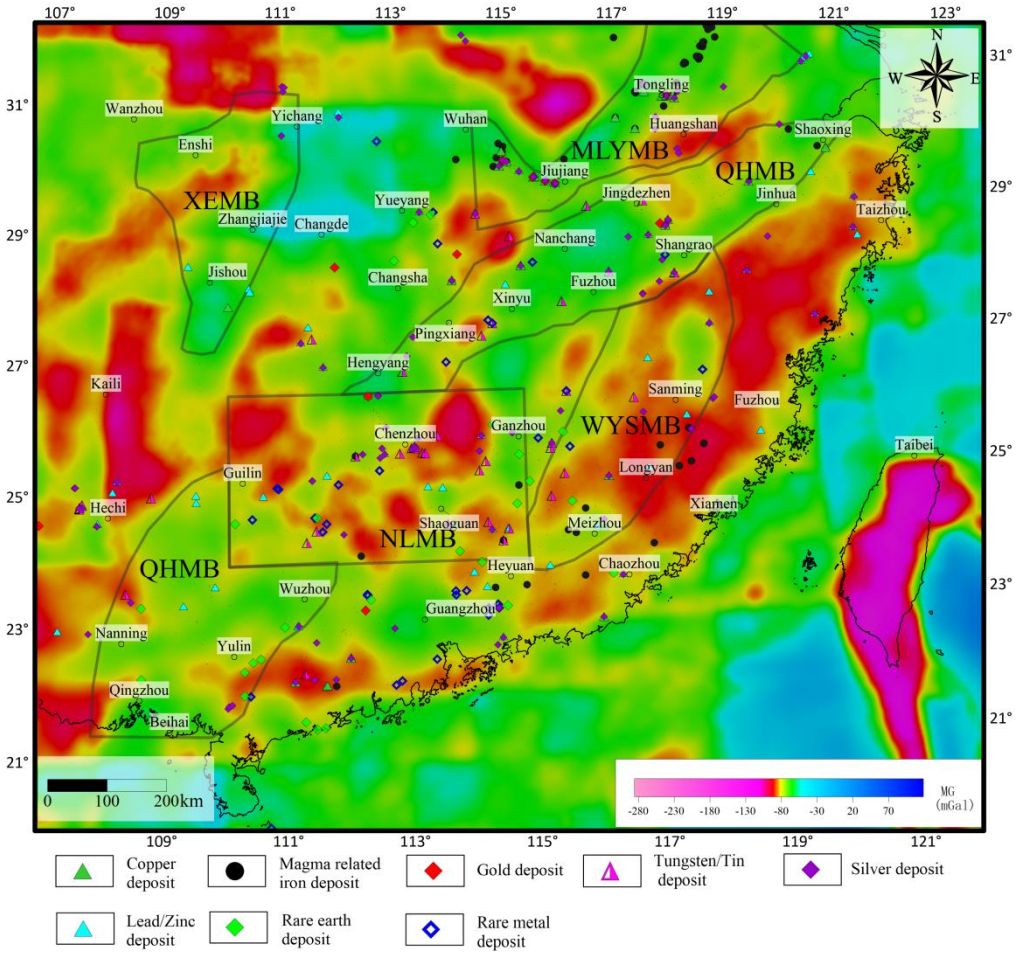

Figure 5. Mantle gravity anomalies of South China

The isostatic gravity anomalies can be obtained by subtracting the isostatic gravity correction values from Bouguer gravity anomalies. In this paper, the isostatic gravity correction values were calculated by the Fast Forward Formula of the gravity field in frequency domain improved by Feng et al. (Parker, 1973; Feng et al., 1985, 1986a, 1986b, 1987). ETOPO1 elevation data were adopted for the terrain. According to Crust1.0 model information, the density of the crust and mantle, as well as the crust-mantle density contrast in the research area, were statistically calculated and the results are as follows: the average density of continental crust, oceanic crust, and the mantle are 2.824 g/cm^3, 2.877 g/cm^3, and 3.3g/cm^3, respectively. Accordingly, the

crust-mantle density contrast is 0.476g/cm^3 in continental zones and is 0.433g/cm^3 in oceanic zones. The average Moho depth is 34.647 km in continental zones and 23.925km in oceanic zones. The average elevation in continental zones is 395 m, and the average water depth in oceanic zones is 646m. The isostatic gravity anomalies in SC were calculated (Figure 6) using the Bouguer gravity anomalies taken as the Bouguer gravity anomalies corrected for the sediment effect of SC that had been corrected in a spherical coordinate system (Figure 4).

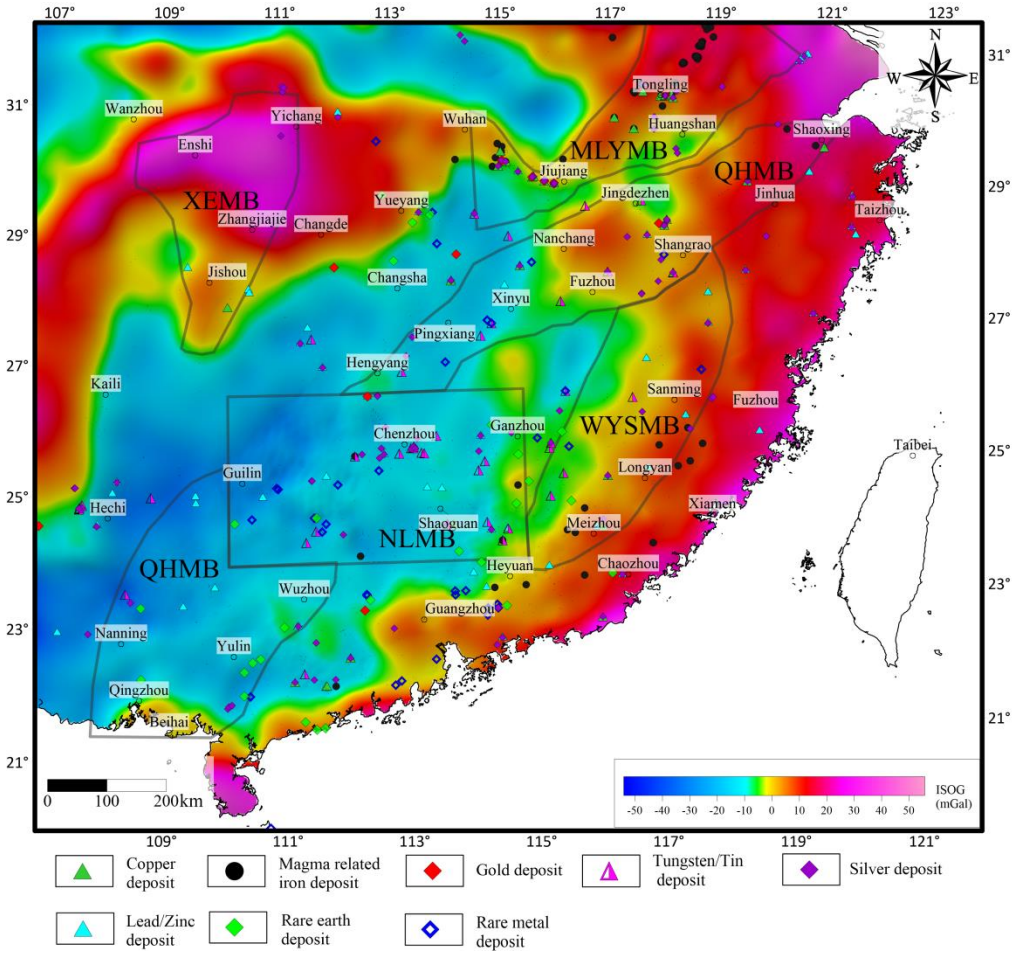

Figure 6. Isostatic gravity anomalies of South China

Presently, the majority of geophysicists tend to interpret an area with isostatic gravity anomalies close to zero or not exceeding a certain threshold-generally considered to be ±20 mGal (Cheng et al., 1985)-as an area where the crust has reached an equilibrium state (Zhang et al., 2003). However, in this paper, it is considered to be incomprehensive to determine whether or not the crust is in an equilibrium state solely according to the amplitude of the anomalies. The reasons are as follows. First, the isostatic correction is only to correct the compensation effect of crustal depth. Second,

448 the isostatic models are not perfect at present, and most especially, it is difficult to
449 determine the isostatic parameters. As a result, certain differences exist between two
450 different models and even in one model with different parameters. As a result, the
451 isostatic gravity anomalies calculated are not necessarily accurate. Therefore, in this
452 paper, the conclusion about whether or not the crust is in an equilibrium state was
453 inferred from the gradient of isostatic gravity anomalies. This means that the crust in a
454 certain area can be considered to be in an equilibrium state if the isostatic gravity
455 anomalies vary gently in the area, even though the amplitude of the anomalies is
456 relatively high. On the other hand, the crust in an area can be considered to be in a
457 non-equilibrium state if the isostatic gravity anomalies in the area feature low
458 amplitude but high or intense gradients.

459 Based on the preceding principle, it was discovered that the crust in most areas of
460 the research area had reached an equilibrium state (Figure 6). Meanwhile, several areas
461 with negative isostatic gravity anomalies, and several areas with positive isostatic
462 gravity anomalies were determined. The former areas are mainly distributed in Dabie
463 orogenic belt and Yangtze-Cathaysian junction belt. In the eastern segment of the
464 Dabie-Qinling orogenic belt, the closer the areas to the hinterland of the orogenic belt,
465 the lower the isostatic gravity anomalies, and they are gradually reduced from -20
466 mGal in the southeastern part to less than -30 mGal in the northwestern part of the
467 orogenic belt. This indicates that the crust in Qinling-Dabie orogenic belt has not yet
468 reached an equilibrium state, and excessive crustal materials are compensated (i.e., the
469 crust has penetrated into the mantle at a high degree, and this is consistent with the
470 Moho depths calculated as shown in Figure 4). Another area with apparent negative
471 isostatic gravity anomalies lies in the central part of the research area in NE trending. It
472 shrinks from the Nanning-Hechi area in the southeastern part towards the northeast in
473 the shape of a trumpet mouth, and extends to Jingdezhen-Huangshan area after passing
474 through Guilin, Yongzhou, Pingxiang, and Nanchang. The amplitude of the negative
475 isostatic gravity anomalies in this area has also decreased from the southwest to the
476 northeast. It gradually changes from less than -30 mGal in Nanning area to less than
477 -20 mGal in Pingxiang area, and then further to -5 mGal in Jingdezhen-Huangshan
478 area. The morphology formed by negative isostatic anomalies in this area is basically
479 consistent with that of Poisson’s ratio in this area acquired by broadband seismic
480 observation (He et al., 2013; Zhang et al., 2019). Low Poisson's ratio indicates the

following two types of tectonic setting in general: (i) tectonic compression environment, where felsic rocks tend to more likely form nappe structures or folds than mafic rocks under the same temperature and pressure conditions, thus causing the ratio of P- to S-wave velocity of the crust to decrease with the increase in crustal thickness; (ii) thinning of some basic rocks in the lower crust subject to delamination, thus resulting in the decrease in the Poisson's ratio of the crust. In this paper, by combining Poisson's ratio results, it is believed that the negative isostatic gravity anomalies reflect the crustal thickening caused by the collision juncture belt between YB and CB and subsequent delamination, both of which led to the negative isostatic gravity anomalies in the research area. Therefore, the negative isostatic gravity anomalies in the research area are mainly distributed in JNO, i.e., the juncture belt between YB and CB. On the contrary, it is also practicable to trace the boundary and scope of JNO according to the distribution of negative isostatic gravity anomalies. Based on this, the northern boundary of JNO is determined to be the Hechi-Kaili-Huaihua-Yiyang-Xianning-South Jiujiang-Huangshan Mountain area, and the southern boundary is determined to be distributed along Qinzhou-Yulin-Wuzhou-Chenzhou-Ji'an-Shangrao area. Positive isostatic gravity anomalies are present in local areas in JNO, such as Nanchang, Ji'an, and Hengyang. This may reflect the late activities in JNO, which caused the Moho upwelling in local areas and further formation of high isostatic gravity anomalies in the local areas.

The positive isostatic gravity anomalies in the research area are mainly distributed in the southeast coastal areas and the southern margin of YB. The high isostatic gravity anomalies in the southern margin of YB are distributed along Enshi-Yichang-Wuhan-Jiujiang-Anqing area. They are basically distributed along with the Wuling uplift in an arc shape in the western section of this area and along the Yangtze River in Yichang area. They are distributed in the shape of an NW-trending belt in Hubei. Then their distribution is suddenly changed to NE trending in the Jiujiang-Huangmei area, and then is in a radial shape in a gradually enlarged area between northern Lujiang and southern Qingyang. The area along the Yangtze River is considered by various geophysical exploration to feature shallow Moho, and the mantle in this area relatively uplifts. This ascertained the deficit in crustal material compensation reflected by the high isostatic gravity anomalies. The areas with high isostatic gravity anomalies along the southeast coastal areas are located in the eastern

514 part of Guangzhou-Huizhou-Meizhou-Longyan-Sanming area, wide in the north and
515 narrow in the south. This may reflect the influence of the NE-trending subduction of the
516 Paleo-Pacific Plate on the crust.

517 *3.5 Magnetic basement depth*

518 The magnetic basement mainly reflects the burial depth of the top of the magnetic
519 layer. The study will help to understand the distribution of crystalline basement, deep
520 intrusions, ore-transmitting pathways, and basement fault structures, thus providing
521 useful information about the deep background of metallogenic belts. There are many
522 magnetic interface inversion methods, which can be roughly categorized into
523 unconstrained inversion and constrained inversion. The former include tangent
524 methods and matched-filtering methods, while the latter includes the inversion based
525 on prior models. However, some of these methods can only determine the burial depth
526 of the top or center of a single magnetic body, and some of them require many prior
527 geological and physical information. In this paper, the burial depth map of the magnetic
528 basement in SC (Figure 7) was calculated by the source parameter imaging (SPI)
529 (Thurston and Smith, 1997; Thurston et al., 2002) method using the EMAG2 of RTP
530 magnetic anomalies in SC (Figure 3).

531 The magnetic basement depth also reflects the intensity of magmatic activities to a
532 certain extent. The shallow magnetic basement indicates previous intense magmatic
533 activities in the shallow crust, and the footprints left by the alteration activities of
534 magma and fluids were retained. It can be seen from Figure 7 that the burial depth of
535 the magnetic basement in SC tends to increase from the southeast to the northwest
536 gradually and is distributed in cloddy shapes in local areas. Moreover, high burial
537 depth is also distributed in some shallow-background areas and vice versa. In general,
538 with F2 as the boundary(Figure7), the burial depth of the magnetic basement in the
539 north is high. This indicates weak magmatic activities in YB-the feature of a cold block,
540 and thus also indicates that F2 serves as a regional boundary. The band with high burial
541 depth along F1 is distributed in the shallow magnetic basement. Its southeastern part is
542 shallow and distributed intensively and continuously, indicating that this part is the CB
543 with frequent magmatic activities. In the narrow zone between the northern part of the
544 band and F2, the burial depth of the magnetic basement is alternatively high and low.
545 These characteristics of different shapes and intensities correspond to the distribution

range of different blocks. They serve as magnetic evidence that the area to the north of F2 is YB, the area to the south of F1 is CB, and the area between F1 and F2 is the juncture belt of YB and CB (i.e., the JNO).

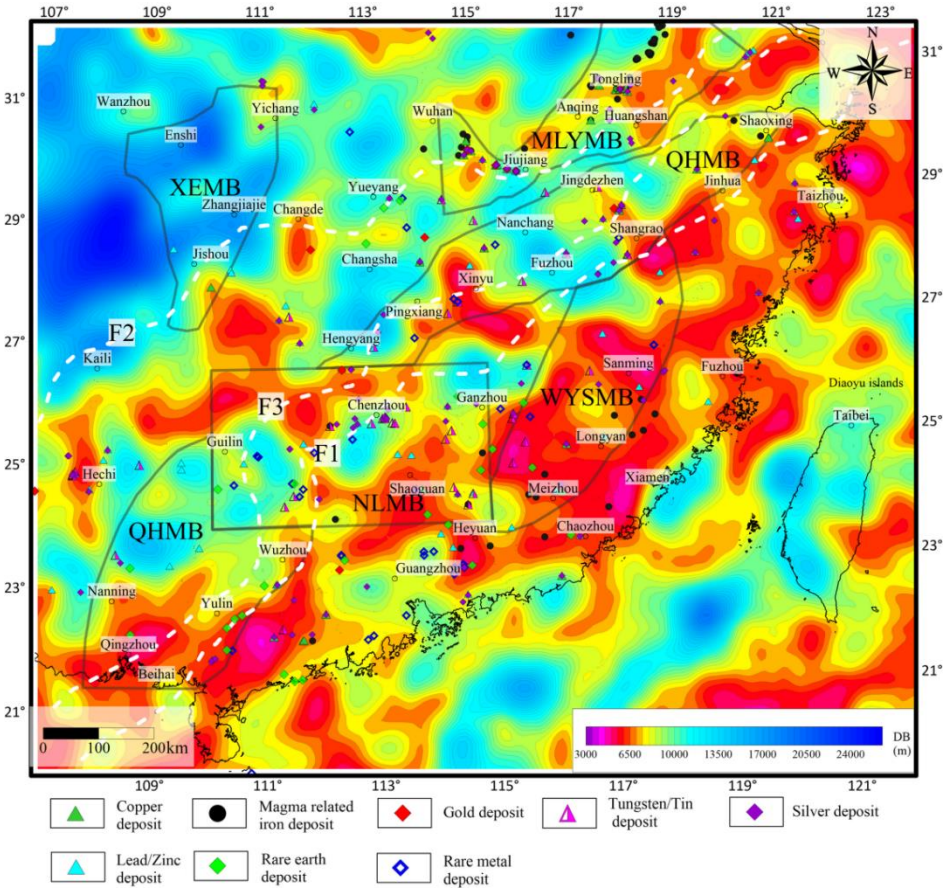

Figure 7. Magnetic basement depth of South China
(F1: the southern boundary of Jiangnan orogenic belt, F3: the northern boundary of Jiangnan orogenic belt)

3.6 Lineament structure

Owing to the difference in physical properties such as density or susceptibility between the two sides of a geological boundary, the gravity and magnetic anomalies near a geological structure boundary are present in the form of gradient zones, which are the boundaries of field sources. Therefore, the main method of extracting the information about gravity and magnetic structures is to extract field source boundaries from the gravity and magnetic anomaly map (Zhang et al., 2015). The common practice is to enhance the information of field source boundaries in gravity and magnetic anomalies, and then determine the positions of the boundaries by a certain edge detection method (Guo et al., 2015). There are many methods of edge enhancement and

563 detection of gravity and magnetic anomalies, such as tilt angle derivative method, tilt
564 angle derivative and horizontal gradient method, and theta-map method. However,
565 different processing results will be achieved by these methods, even for the same group
566 of gravity and magnetic data since these methods are based on different principles and
567 different applicable preconditions. Therefore, it is necessary to select the most suitable
568 detection method by comparing and analyzing the detection effects of various methods.
569 Usually, in the process of gravity and magnetic anomaly interpretation of different
570 regions or different geological backgrounds, it is also necessary to screen a detection
571 and enhancement method that well suits actual geological conditions by comparing and
572 analyzing the results acquired by various methods. In this way, a reasonable geological
573 interpretation can be made by combining comprehensive analyses of existing data.
574 After comparing the widely used total horizontal gradient method, tilt angle derivative
575 method, theta-map method, and multiscale edge detection method Worms through
576 model testing, Yan et al. (2015) found that Worms is more suitable for edge extraction
577 of large-scale gravity and magnetic data and has played an active role in tectonic
578 information extraction of MLYMB (Yan et al., 2011).

579 In this paper, the edge detection results of the east of SC were obtained by
580 multiscale edge detection for both Bouguer gravity anomalies (Figure 2) and RTP
581 satellite magnetic anomalies (Figure 3). The multiscale edge detection results of
582 satellite gravity anomalies in the east of SC are shown in Figure 8, from which it can be
583 seen that the Worms lines are distributed in linear shapes in general and in the shapes
584 of rings and semi-rings in local areas. The linear Worms lines reflect the boundaries of
585 faults and blocks. The tectonic lines denoting the deep crust are distributed in NNE
586 trending in most areas, mainly in NW trending in the western part and in NNE trending
587 in west Guangxi. Some tectonic lines denoting the shallow crust vary greatly in
588 direction, reflecting the complexity of the structures in the shallow crust. The ring and
589 semi-ring-shaped Worms lines mainly indicate the boundaries of intrusions and basins.
590 The reliability of boundaries determined by Worms can be ascertained by the
591 amplitude intensity of edge detection for gravity anomalies (Figure 9a). The sections
592 with intense amplitude signals indicate a strong possibility for the existence of density
593 body boundaries. The intense amplitude signals of edge detection in SCB are also
594 found to be mainly in NE trending, indicating that the deep structures in SCB are
595 mainly in NE trending.

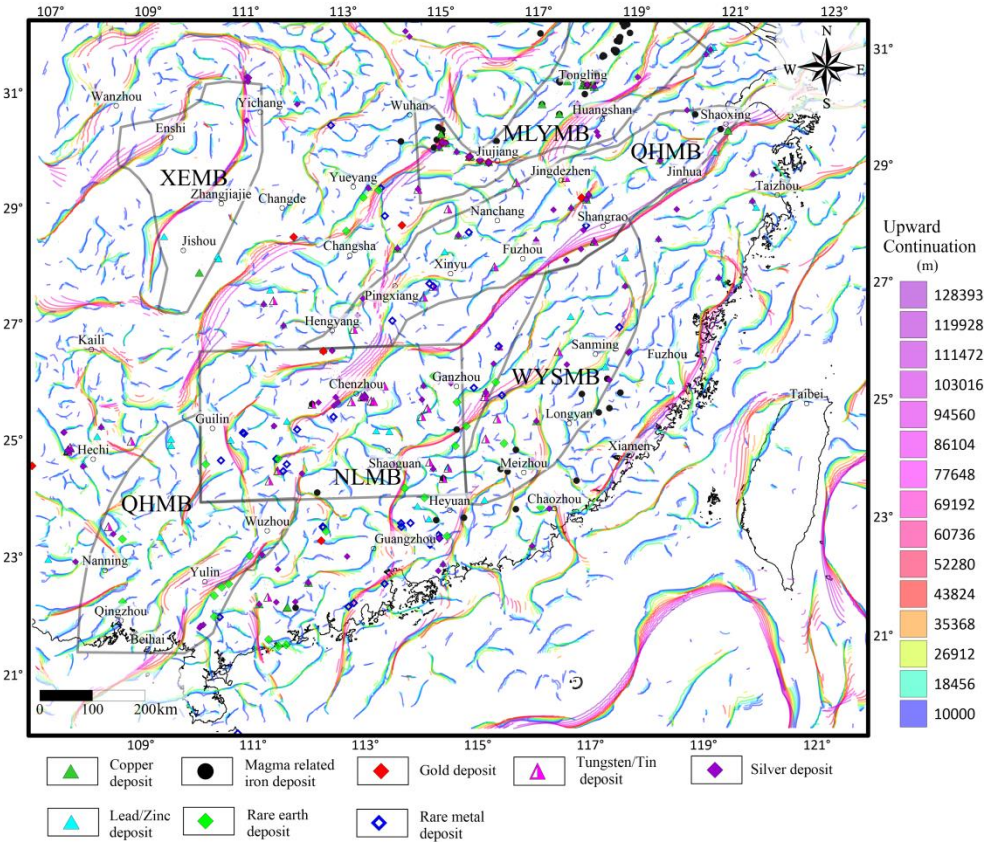

Figure 8. Multiscale edge detection results of Bouguer gravity anomalies in South China

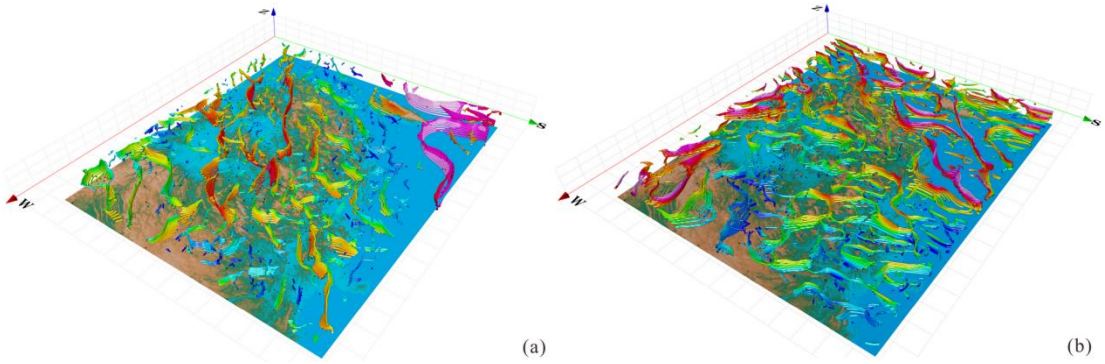

Figure 9. Persperctive view of amplitude intensity of multiscale edge detection results of Bouguer gravities (a) and EMAG2 after RTP (b) of South China

(The lines colors from blue to purple indicate weak to strong amplitude intensity of detection lines; the base map is ETOPO1 digital elevation map)

The edge detection results of RTP satellite magnetic anomalies in the east of SC are shown in Figure 10. The Worms lines reflect the boundaries of different magnetic bodies. The linear Worms lines reflect the boundaries of magnetic geological bodies or faults, while the ring-shaped Worms lines mainly reflect the boundaries of intrusions

(concealed intrusions) and volcanic basins. The Worms lines of CB, YB, and Dabie orogenic belt have quite different characteristics and shapes. The Worms lines of YB are mainly linear and in NE trending, mainly reflecting the boundaries of the strata inside the block. As for the Worms lines of CB, ring-shaped Worms lines are widely distributed besides linear Worms lines. Most especially in the eastern part of CB, ring-shaped Worms lines representing different scales and different depths are all present. Most of these ring-shaped structures reflect the distribution of intrusions and concealed intrusions. As for the Worms lines of the Dabie orogenic belt, the NE-trending Worms lines on both sides of the orogenic belt denote Tan-Lu fault, and two NW-trending boundaries denote Xiangfan-Guangji fault and Xiaotian-Mozitan fault. The reliability of boundaries determined by Worms can be ascertained by the amplitude intensity of edge detection for RTP satellite magnetic anomalies (Figure 9b). The sections with intense amplitude signals indicate a strong possibility for the existence of the boundaries of magmatic bodies.

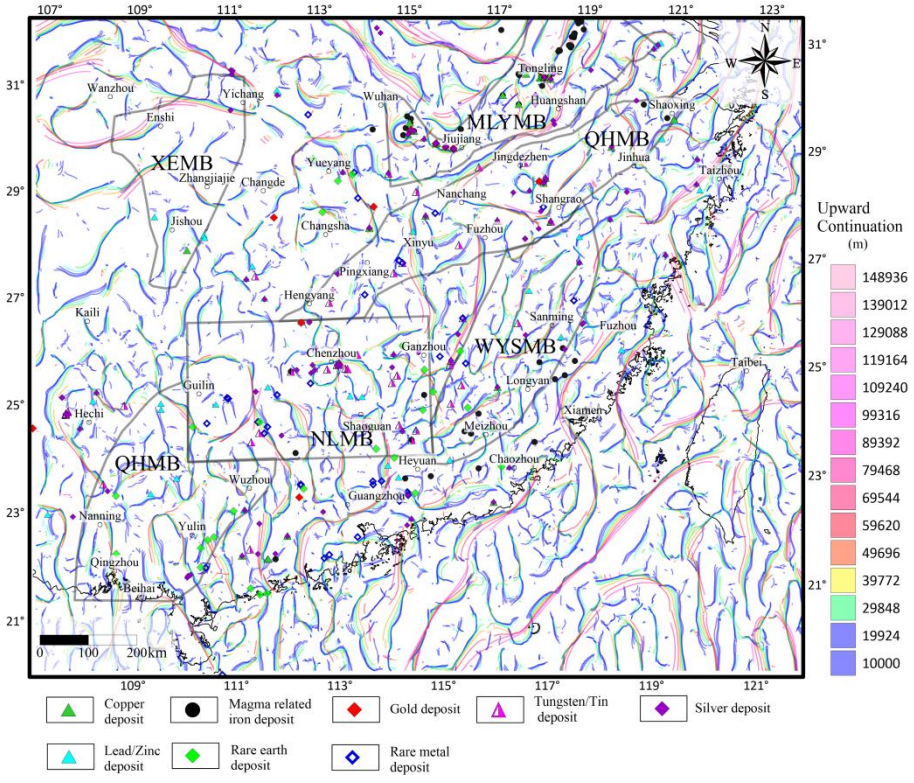

Figure 10. Multiscale edge detection results of EMAG2 RTP magnetic anomalies in South China

The tectonic framework in the east of SC was determined based on multiscale edge detection for gravity and magnetic anomalies, isostatic gravity anomalies, and

627 magnetic basement depth (Figure 11). In general, the tectonic lines in SC are primarily
628 in NE-SW trending and secondarily in NW-SE trending. It can be seen from Figure 8
629 that there is a continuous obvious Worms lines along with Shaoxin-Jinhua - Shangrao -
630 north-Ganzhou – Chenzhou – Wuzhou - Yulin - east Beihai. The northeastern section
631 and the northern section of the Worms lines coincide with Jiangshan-Shaoxing fault
632 and Chenzhou-Linwu fault, respectively. Therefore, the traced fault F1 is considered to
633 be the southern boundary of the Qingzhou-Hangzhou juncture belt. There is a
634 continuous lineament along with south Jingdezhen – Fuzhou – Xinyu – Pingxiang –
635 Hengyang – Guilin - west Wuzhou – Qinzhou. It is considered that the fault F3 can be
636 formed by intermittently tracing this pencil of Worms lines, i.e., the northern boundary
637 of the Qinzhou-Hangzhou juncture belt. It can be seen from the amplitude intensity of
638 the Worms lines (Figure 10a) that F1 has greater cutting depth and a more complete
639 shape than F3. The ratios of P- to S-wave velocity of the crust in YB and CB are found
640 to be relatively high from Poisson's ratio distribution obtained from natural seismic
641 tomography (Zhang et al., 2019, Chen et al., 2019, He et al., 2013), while the juncture
642 belt between YB and CB shows significantly low ratios of P- to S-wave velocity.
643 Furthermore, the southern boundary of high anomalies of the ratio of P- to S-wave
644 velocity basically coincides with the inferred F1. All of the aforementioned detection
645 results indicate that F1 may be the main boundary resulting from the subduction of CB
646 towards YB (i.e., the southern boundary of JNO). It can also be seen from Figure 9 that
647 there exists another obvious Worms lines F2 from Huangshan to Jiujiang and Yueyang,
648 whose amplitude intensity is equivalent to that of F1. Based on this, as well as the
649 multiscale edge detection results of satellite magnetic anomalies (Figure 10),
650 magnetotelluric apparent resistivity, and ratio of P- to S-wave velocity from broadband
651 seismic (Yan et al., 2019), it is inferred that Huangshan - Jiujiang - Yueyang - Changde
652 - Jishou– Kaili area is the northern boundary of JNO. F4 is inferred to be
653 Changle-Nan'ao fault.F5 is inferred to be Zhenghe-Dapu fault，it divides the CB into
654 the eastern part and western part, and the eastern part is a coastal volcanic area.F6 is
655 mainly Heyuan-Shaowu fault. F7 is Jianshi-Pengshui fault, F8 is Qiyueshan fault, F9
656 may be a part of Huayingshan fault, and F12 is the newly inferred Bazhong-Yichang
657 fault (partially coinciding with Tianyangping-Jianli fault). F10 is Tan-Lu fault, F11 is
658 Yangtze River deep fault, F13 is Xiangfan-Guangji fault, F14 is Xiaotian-Mozitan fault,
659 and F15 is inferred to be Tongling-Taizhou fault.

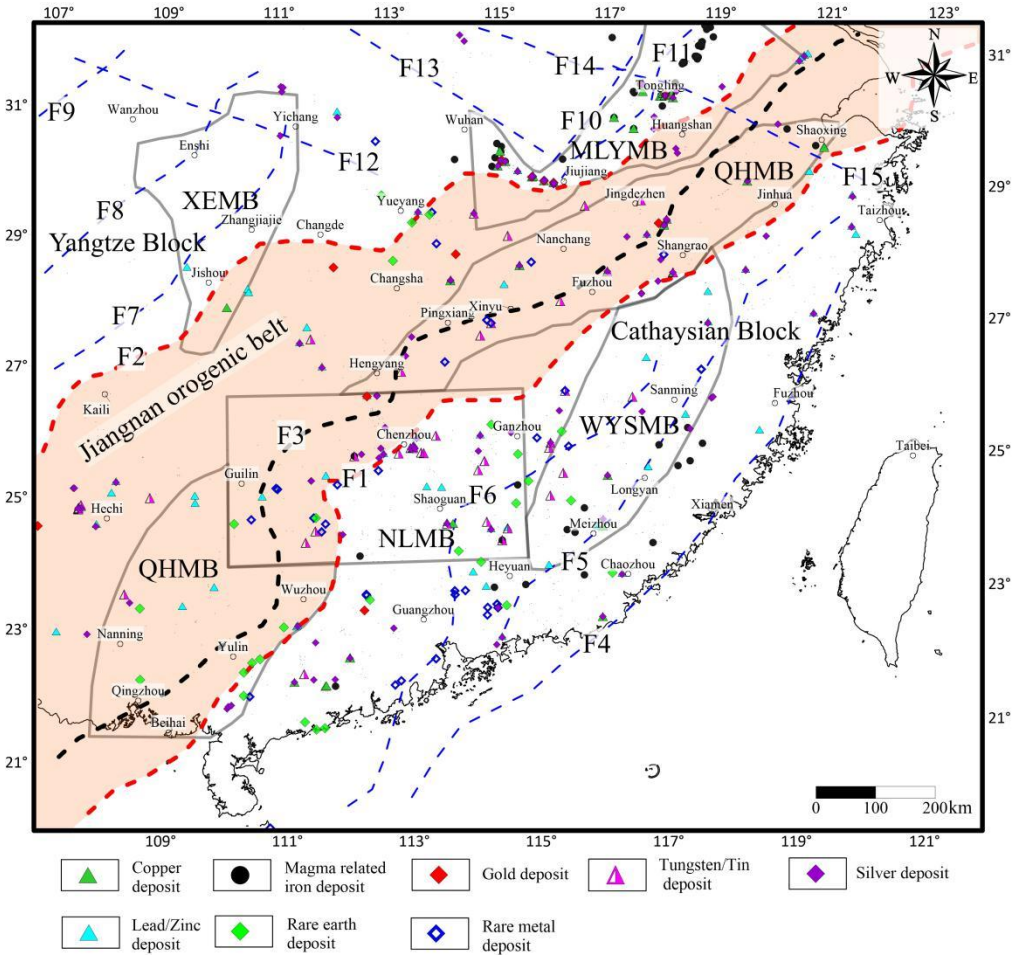

Figure 11. Tectonic framework of South China inferred from gravity and magnetic data procession

3.7 3D density and susceptibility model

The 3D gravity and magnetic physical properties inversion can be used to establish 3D models of underground density and susceptibility, thus proving relevant information about physical properties related to the underground material composition. The basic principle of this is as follows. The area of the field source is broken down into smaller units (cuboid or cube units). The morphology of the units remains unchanged, while the physical properties of the units vary during the inversion. For this reason, the scope of the field source can be determined according to the changes in the physical properties. In this paper, the physical properties inversion programs UBC Mag3D and Grav3D developed by the University of British Columbia in Canada were applied. Their core algorithm is based on the gravity and magnetic anomaly inversion algorithm proposed by Li et al. (Li, 1996, 1998). They are equipped with an interface used to put constraints of prior information, thus making it practicable to

carry out the inversion with prior constraints (Williams, 2008).

The same mesh division file was used in both 3D gravity inversion and 3D magnetic physical properties inversion, and the details are as follows. A cell is 5,000 m long in the horizontal direction, and its thickness in vertical direction gradually increases from 500 m to 1,000 m, 2,000 m, 5,000 m, and 10,000 m as the depth gradually decreases. To minimize the edge effect, the mesh was extended by 35,000 m in the directions of east, south, west, and north individually. In this way, the underground of SC was divided into 155 (in north-south trending) × 155 (in east-west trending) × 35 (vertical) = 4,385,502 regular cells, which fill in the whole lower half of SC. 3D gravity inversion was performed in Chifa mode, with the smoothing coefficient of 0.4 and the density range of -1–1 g/cm^3. A 3D density model was obtained by the inversion through depth weighted calculation (Figure 12a). The depth weighted method under the Generalized Cross-Validation (GCV) model was used for magnetic inversion in the value range of 0–1 SI. In this way, a 3D susceptibility model was also obtained (Figure 12b).

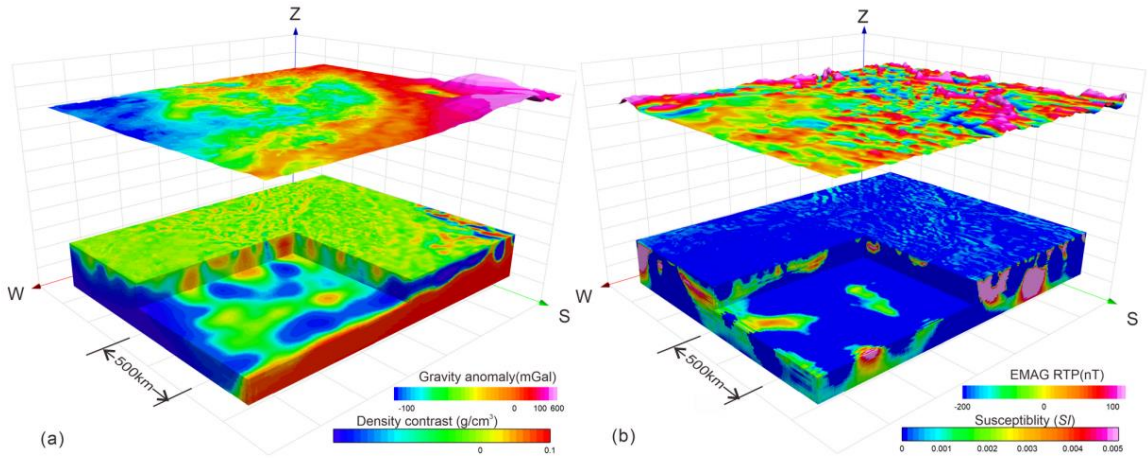

Figure 12 Persperctive view of 3D gravity inversion results (a) and 3D magnetic inversion results (b) of South China

(topper is gravity or EMAG RTP anomalies，bottomer is density contrast or susceptibility model）

4 Discussion

4.1 Source zones of mineral systems in metallogenic belts in South China

Different types of mineral systems have different source zones. For instance, the source zones of sandstone-type uranium deposits may be sedimentary strata (paleo-weathered crust), in which the uranium deposits are enriched through groundwater circulation. In contrast, the mineral systems associated with magmatic-hydrothermal activities may have multi-level source zones, which may be the sub-continental lithospheric mantle (SCLM), LAB, or the crust-mantle boundary (basic magma underplating belt, i.e., the Moho) in deep strata, or large magma chambers in shallow strata. In subduction zones, for example, mantle wedges were transformed by dehydration and melting of oceanic crusts, leading to the enrichment of metals (Mungall and E., 2002; Hou et al., 2015). Then the magma generated underplated the mantle-crust boundary and was transformed into ore-bearing magma through melting, assimilation, storage, and homogenization (MASH). In recent years, some experts argued that the structure of SCLM plays an essential role in controlling the formation of super-large deposits (Griffin et al., 2013) and emphasized that the boundary, composition, and fertility of continental plates, as well as the evolution of SCLM, may serve as critical factors that control the "source zones" of mineral systems. In this paper, possible source zones of the mineral systems in major metallogenic belts of SC were analyzed by combining the characteristics of vertical structures such as the Moho calculated based on the gravity and magnetic data.

4.1.1 MLYMB

As indicated in the Moho depth map calculated with gravity data (Figure 4), the Moho in MLYMB area consists of one uplift and two subsidence areas, with the uplift lying between the two subsidence areas, and the MLYMB lies in the uplift belt of the Moho. The mantle gravity anomalies (Figure 5) also indicate that MLYMB is located in the uplift belt of the mantle. Meanwhile, the ore concentration areas in MLYMB clearly correspond to the uplift of the ground, and they are mainly distributed in the ridge and southern mantle slope of the mantle uplift. As shown from the Moho depth isolines, the two sides of the mantle uplift of MLYMB are different in steepness and width, and the gradients of the isolines are high on the northern side and low on the southern part. This suggests that, compared to the northern mantle slope, the southern mantle slope is wider and has a larger volume and a larger contact area with the lower crust. Therefore, it provides longer crust-mantle interaction in larger space, creates more opportunities to extract metallic elements from the crust, and makes it easier for

732 the formation of deposits.

733 Meanwhile, the lower crust was continuously roasted owing to the large
734 crust-mantle contact area. As a result, part of the lower crust was melted, and
735 delamination was more likely to take place, thus intensifying the crust-mantle
736 interaction (Rudnick, 1995). Furthermore, the roasting also resulted in the melting of
737 the lower crust far from the mantle ridge. As a result, the magma dominated by
738 crust-derived magma was generated. Then it rose and emplaced and became
739 intermediate-acid intrusions, forming hydrothermal or porphyritic polymetallic
740 deposits in some areas. This is the fundamental reason why there are a large number
741 of Pb and Zn deposits in the areas on the southern mantle slope, such as Qingyang and
742 Guichi. On the other hand, the northern mantle slope is narrow and thus has a
743 comparatively small crust-mantle interaction area and crust-mantle material exchange
744 space. Therefore, it is difficult for metal deposits to be formed in this area (Figure 13).
745 According to the comparison of the isostatic gravity anomalies with the distribution of
746 metal deposits in MLYMB (Figure 6), nearly all deposits are distributed in the areas
747 with positive isostatic gravity anomalies except for the deposits in Jiujiang and the
748 southeast Hubei, which are distributed on the southern side of the areas. Most
749 importantly, the deposits are more likely to take place on the margin of locally deeper
750 parts in the areas. Overall, there is a clear positive correlation between positive
751 isostatic gravity anomalies and the occurrence of metal deposits.

752 For these reasons, it is considered that the Fe and Cu mineral systems in
753 MLYMB have multi-level source zones. The initial-level source zone is the enriched
754 mantle, which is formed owing to the thinning of the lithosphere and the deformation
755 caused by the fluids in the asthenosphere. Some of the enriched mantle melted and
756 underplated, and were mixed with the materials in the lower crust, and then formed
757 metallogenic magma containing abundant Cu and Fe through MASH. Owing to the
758 influence of spatial positions, time, and the injection proportion of mantle-derived
759 magma, different series of magma and related deposits were formed in the
760 metallogenic belts during the formation and evolution of the source zones.

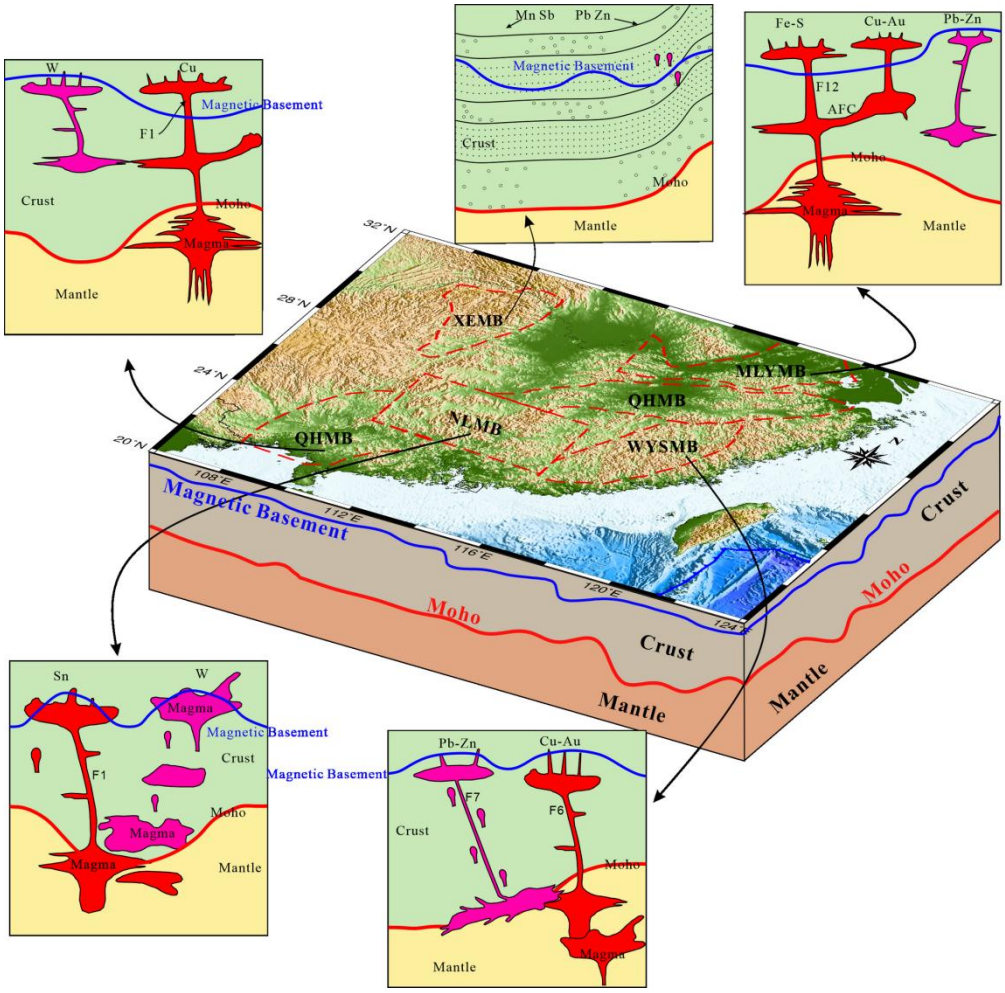

Figure 13. Schematic diagram of the main control factors of the mineral system of main metallogenic belts in South China

4.1.2 NLMB

NLMB is one of the most important areas in the world where Sn and W deposits are distributed in a concentrated way, with W deposits mainly distributed in the eastern segment and Sn deposits in the western segment. The Moho in NLMB is 35–39 km deep (Figure 4), and it deepens gradually from east to west and uplifts slightly from Shaoguan to Chenzhou, reflecting the thickening of the crust in this belt. NLMB features negative isostatic gravity anomalies, indicating an excess of crustal material compensation in this belt. This means that the crust has penetrated into the mantle at a high degree, also reflecting that the crust is thickened. It is generally believed that the areas with low mantle gravity anomalies indicate the thickening of the crust or the presence of low-density anomaly zones in the crust/upper mantle formed owing to high temperature or partial melting (Corimer et al., 1995). Given the fact that NLMB

features low mantle gravity anomalies (Figure 5), as well as the Moho depths (Figure 4) and isostatic gravity anomalies (Figure 6) in this belt, it is believed that NLMB features not only crust thickening but also the presence of melted low-density bodies in the upper mantle. The magnetic basement of NLMB is presented in the shapes of strips and blocks with different depths (Figure 7), and the W and Sn deposits are mainly distributed in areas with shallow magnetic basement and the gradient belts of the magnetic anomalies. The magnetic basement of NLMB suggests the traces of magmatic activities to a great extent. Therefore, it can be inferred that the magma upwelling from the deep part of NLMB was blocked by the thickened crust and then remelted, and thus were mixed with more crust-derived materials. After intruding upwards, the high-temperature and high-pressure magma were trapped in the upper crust and then underwent remelting with materials in the upper crust and metasomatization of metallogenic elements, resulting in the mixing and emplacement of the magma dominated by crust-derived magma. As a result, metallogenic elements were enriched near the Nanling area, and large deposits were ultimately formed, including Xitian Sn deposit, Shizhuyuan Sn deposit, Xianghualing Sn deposit, Yaogangxian W deposit, Xintianling W deposit, Furong Sn deposit, and Baiyunxian W deposit (Figure 13).

4.1.3 QHMB

QHMB is located in the zone where two paleo-continental blocks, namely CB and YB, collided and spliced together. It experienced multiple stages of mineralization, such as Yanshanian, Caledonian, and Jingningian, and, as a result, a huge number of polymetallic deposits such as Cu, Au, and W deposits were formed in this area. It can be divided into the eastern segment and western segment according to spatial and metallogenic features, with NLMB in its middle as the boundary. The eastern segment is characterized by Cu and Au mineralization, and many large-medium and superlarge Cu-Au polymetallic deposits have developed in this segment. In contrast, the western segment features mineralization of rare metals such as Au and Ag, with several rare metal deposits being developed in this segment (Figure 1).

The Moho in QHMB generally uplifts in NE-SW trending in banded shapes and is disconnected by the mantle subsidence area of NLMB (Figure 4) in the middle part of QHMB. It is generally believed that the areas with high mantle gravity anomalies

reflect the thinning of the crust or the presence of high-density anomaly zones in the upper mantle (Corimer et al., 1995). The mantle gravity anomalies are high in QHMB in general (Figure 5), which also proves that QHMB is located in the mantle uplift areas. The eastern segment of QHMB features positive isostatic gravity anomalies. Therefore, it is inferred that in the early stage of early Yanshanian, the Paleo-Pacific Plate subducted towards the SCB, during which the compressive stress on the continental margin produced remote effects within the continent. As a result, the suture zone boundaries between various blocks in the Qingzhou-Hangzhou juncture belt were activated, causing the melting of the thickened lower crust accompanied by delamination. Then the magma was mixed with more mantle-derived materials and formed massive type-I granitic magma, thus providing material sources for Cu-Au polymetallic deposits. From the late stage of early Yanshanian to the early stage of late Yanshanian (160–125 Ma), the eastern segment of QHMB underwent intense flat-slab subduction, and the tectonic background of entire SC was gradually transformed from compress to extension as the subducting angle increased. Next, massive materials in the asthenosphere upwelled, and flat-slab subduction dehydration led to the melting of mantle wedge and further generation of underplated basaltic magma. This caused the crust to remelt at a large scale and form type-S granitic magma, thus providing material sources for deposits of W, Mo, Nb, Ta, etc. (Liu, 2015; Zhou, 2003). From the early stage of late Yanshanian to the late stage of late Yanshanian (136–100 Ma), as the angle of flat-slab subduction further increased and the extension continued, the basaltic magma intruded into the shallow crust and was mixed with the magma chamber of the crust. In addition, the depleted mantle-derived magma was mixed with the felsic magma formed by the resultant melting of shallow crust materials. Then the mixture was further differentiated and evolved into type-A granites, which possess the diagenetic and metallogenic characteristics of both type-I and type-S granites. The type-A granites were finally enriched in favorable places to form deposits (Liang et al., 2012, 2015).

The western segment of QHMB has experienced multiple cycles of opening-closing tectonic movements since the Neoproterozoic. During the Caledonian movement, Guangxi geosyncline became a folding zone again, and regional metamorphism and fault metamorphism were widely developed, leading to the gradual formation of the southern uplift in the western segment. A series of

brittle-ductile shear zones and thrust nappe structures were developed owing to the fold orogeny during the Yanshanian, providing pathways for magmatic activities and causing joints and fissures to occur in the rocks on both sides of the western segment. Magma intruded upwards along with the structures such as fault fissures and mixed with atmospheric precipitation permeating downwards along the fissures. Then metallogenic hydrotherm was formed after the magma leached the metamorphic rocks and the granites driven by its thermal energy. The metallogenic hydrotherm then caused massive hydrothermal alteration of the surrounding rocks of the fissures it passed by, during which metallogenic elements such as Au and Ag in the rocks were activated, migrated, and redistributed. In this way, polymetallic deposits of rare metals such as Au and Ag were ultimately formed (Wang et al., 2002; Chen, 2010). Therefore, in this paper, it is believed that the source zone of Cu deposits in QHMB, such as Dexing deposit is the mantle while the source zone of W deposits on the margin of the Moho uplift such as Zhuxi and Dahutang deposits is the remelted crust(Figure 13).

4.1.4 WYSMB

WYSMB of Cu, Pb, and Zn is an important metallogenic area in CB. It is next to the eastern segment of QHMB in the north and to the eastern segment of NLMN in the west. It has a unique tectonic environment and a long and complex evolutionary history of structure-magma-metallization in the deep part, which creates favorable metallogenic geological conditions and rich mineral resources. The Moho of WYSMB is deep in general (Figure 4) and shallow locally along the Nanping-Sanming area. WYSMB features low mantle gravity anomalies (Figure 5), indicating that the crust is thick and local melting exists in the upper mantle. The isostatic gravity anomalies are high in the east and low in the west (Figure 6). This indicates that the crust corresponding to thick metallogenic belt underwent remote effects of the subduction of the Paleo-Pacific Plate later, imposing intense crust-mantle interaction on WYS. The shallow magnetic basement in WYSMB implies that magma activities took place frequently in the area, thus forming a large igneous province in east China. Based on the Moho depths and the isostatic gravity anomalies in NLMB, it can be considered that WYSMB features not only crust thickening but also the presence of melted low-density bodies in the upper mantle.

Based on the characteristics of the crust-mantle juncture zone revealed by gravity

and magnetic data, it is believed that, in the late Mesozoic, the local mantle uplift between Meizhou and Longyan underwent delamination in the process of lithosphere thickening, the materials in the asthenosphere upwelled, and the faults or fracture zones served as the pathways for the migration of ore-bearing magma. The new crust was formed as the mantle materials containing Cu and Au elements participated in crust remelting, and the basement rocks in Taoxi uplifted subjected to the crust extension and magma jacking (Chen et al., 2010). The Moho in the northeast of WYSMB is a mantle subsidence area. As indicated by the recent results of plate reconstruction and evidence of Haishan K-Ar age, the Paleo-Pacific Plate subducted into the continental lithosphere in southeast China along with NWW trending in the late Yanshanian (145–100 Ma), during which the oceanic plate itself underwent delamination-rotation-retreating. Meanwhile, the mantle materials upwelled and intruded into the crust through large deep fractures, then they melted the crust materials in the low-speed bodies of the lower crust, and finally intruded into the upper crust through the deep fault (Ji, 2018). This indicates that the diagenism and mineralization in WYSMB are mainly related to the interactions between materials in the crust and the mantle, with crust-derived materials forming the deposits mainly consisting of W and rare earth and mantle-derived materials forming polymetallic deposits such as Cu and Au (Figure 13).

4.1.5 XEMB

XEMB is located on the southeast margin of YB. It is an important reserve and production base of metal mineral resources such as Sb, Pb, Zn, Au, and Mn in China, with measured and initially indicated Zn and Pb resources greater than 8 million tons and prospective Zn and Pb reserves greater than 15 million tons. It boasts the measured Sb reserves that account for more than 70% of the total Sb reserves in the world, thus serving as a world-renowned Sb capital, and furthermore, it enjoys the potential for further prospecting of Sb (Zhou et al., 2014). The Moho in XEMB is about 33–38 km in depth, gradually rising from west to east. It can be divided into two parts, namely the eastern uplift area and western subsidence area, according to the relative distribution of mantle uplift and subsidence (Figure 4). It features high mantle gravity anomalies in general (Figure 5), which also indicates that the crust in XEMB is thick in general. On the other hand, the Zunyi-Qianjiang-Yichang area features low gravity anomalies, showing local mantle uplift. In recent years, multiple diamond

deposits have been discovered in the Yuan River basin, Hunan Province, where positive isostatic gravity anomalies are high (Long, 1999). According to the theory that the mantle serves as the source zone of the diamond, it is believed that diamond formed on the bottom of the lithosphere and on the top of the asthenosphere early in 2–4 Ga, and the far younger kimberlites or lamproites only serves as a medium used to transport diamond-bearing matters formed by the disintegration of the mantle out for mineralization. The metallogenic rules of diamond are generalized to being "old, thick, cold, dry, and brittle" (Long, 1999). "Old" refers to the old and steady platforms and their surroundings; "thick" refers to the thickness of the lithosphere, which was 150–200 km; "cold" refers to the non-existence of plenty of magmatic activities of multiple stages; "dry" means that magma and its surrounding rocks are poor in water, making it possible for melted magma to rise to the maximum height; "brittle" means that the lithosphere is very brittle, thus conducive to fissures occurring from bottom to top. XRMB features positive isostatic gravity anomalies, reflecting local Moho uplift and crust thinning. However, a large tract of Cambrian and Precambrian strata are exposed in most areas of XRMB, indicating the XRMB was an "old, thick, cold, and dry" YB. Then the lithosphere was thinned owing to the crustal isostatic adjustments. As a result, multiple brittle deep faults were formed, and diamond deposits occurred in favorable sections (Figure 13).

The magnetic basement of XEMB is deep in general, which also indicate weak magmatic activities. Based on this, as well as the fact that most Zn and Mn polymetallic deposits in XEMB are of the type of strata-bound sedimentation, it is considered that the source zones of XEMB are mainly the crust.

4.2 Pathways of mineral systems

Mineral deposit geologists have long noticed the controlling of deep faults over the spatial distribution of deposits. For instance, Central Andes porphyry Cu deposit zone in South America, Kalgoorlie Au field in west Australia (Drummond and Goleby, 1993), and Gangdise porphyry Cu deposit belt are all obviously under the control of giant linear structures (i.e., deep faults), which are considered as the "pathways" used in connecting the source zones and sites of mineral systems or considered as the "footprints" left by pathways in metallogenic epochs. The boundaries between these deep faults and blocks are clearly shown from the multiscale edge detection results of

gravity anomalies in SC (Figure 11). As found in the 3D view established by integrating the multiscale edge detection results of gravity anomalies and the density contrast and Au deposit distribution obtained from 3D gravity inversion (Figure 14), most of the Worms lines coincide with the density contrast boundaries, and Au deposits tend to lie along the Worms lines and the density contrast boundaries. As indicated by the fact that both linear structures and density contrast (density gradient) belts are positively correlated with the distribution of the deposits (such as Au and Cu deposits) controlled by mantle-derived components, the Worms lines and the density gradient zones ever serve as the pathways of endogenetic metal deposits in SC, or they are the footprints left by fluid migration. For example, the metallogenic pathways of Fe and Cu deposits in MLYMB are mainly the Yangtze River deep fault in NE trending (F12) and Tongling-Taizhou fault in SE trending (F16) and its secondary faults (Figure 11). The eastern segment of QHMB is mainly controlled by the faults in northeast Jiangxi (the northern segment of F3), the southern segment of QHMB and the NLMB are mainly under the control of the boundary faults of F1, and WYSMB is related to Zhenghe-Dapu fault (F6) and Heyuan-Shaowu fault (F7).

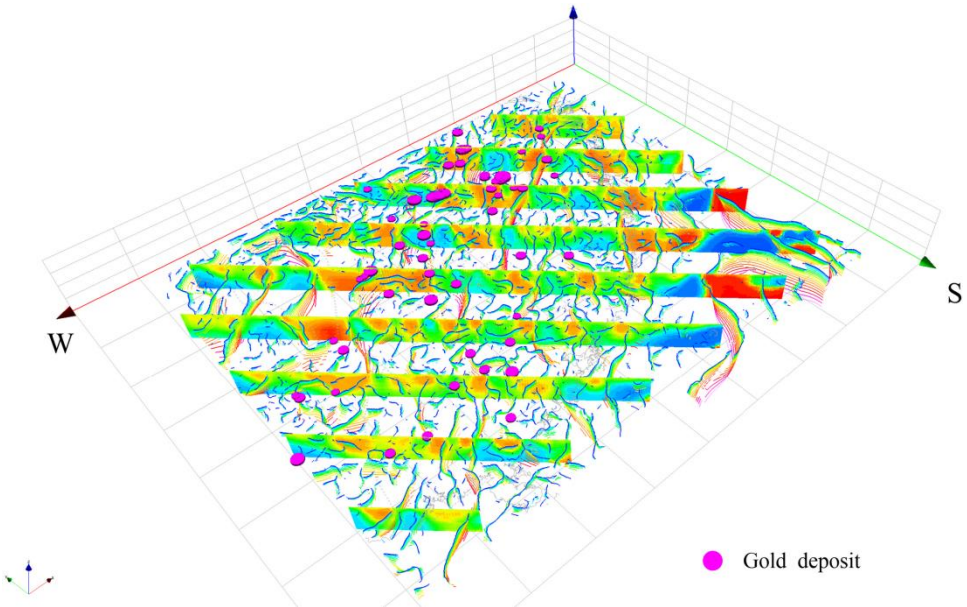

Figure 14. Worms lines from gravity anomalies multiscale edge detection , vertical slice from 3D gravity inversion, and Au deposit location of South China (Vertical grids are vertical slices obtained from 3D density contrast model inversion of gravity data, the lines are multiscale edge detection results of gravity anomalies, the line colors from blue to red represent shallow to deep border depth, and the purple cake shapes represent Au deposit locations)

4.3 Control of intrusions on terminations of mineral systems

The metallogenic materials at the terminations of mineral systems tend to accumulate on "sites" where metallogenic fluids regularly drain, and minerals precipitate. The sites are 0–10 km deep in the upper crust in general, their depth varies with the type of deposits, and their spatial scope tends to be larger than the deposits themselves. A "site" of a mineral system consists of two parts that are spatially related to each other, namely Paleo-fluid reservoirs and mineral depositing space (it is difficult to distinguish between them sometimes). The former is used to supply metallogenic fluids continually and is generally classified into three types: (1) magma intrusions and their surrounding fluid systems; (2) fissure areas with a certain volume that are formed owing to rock fracture; (3) permeable sedimentary aquifers, with the surrounding being closed by lower-permeability layers. The structure and formation process of the "sites" are comparable to the metallogenic process of modern submarine hydrothermal sulfides (or modern volcanic system or hot spring system). In detail, deep magma intrusions drive ore-bearing brine to erupt out of the seabed along faults, and then ore-bearing materials precipitate to form deposits owing to the changes in temperature and physical/chemical conditions. All these three types theoretically correspond to low-density bodies and thus can be analyzed with the density model obtained from 3D gravity inversion. It is difficult to quantitatively analyze the relationship between the physical properties and lithology uniformly in SCB owing to its large scope. However, the qualitative analysis of density and susceptibility can be used to provide bases for the lithological distribution in SCB. As revealed by the distribution of low-density bodies determined by the 3D density model of gravity inversion and the distribution of intrusions determined by ground surface mapping (Figure 15a), the intermediate-acid intrusions that are visible on the continental ground of SCB mostly lie above low-density bodies. Therefore, the low-density bodies can be approximately deemed as large batholiths. Furthermore, the basic intrusions in the ground are mostly located above or next to high-susceptibility bodies (Figure 15b), indicating that the high-susceptibility bodies reflect hydrothermal activities of intermediate-basic intrusions and magma to a great extent.

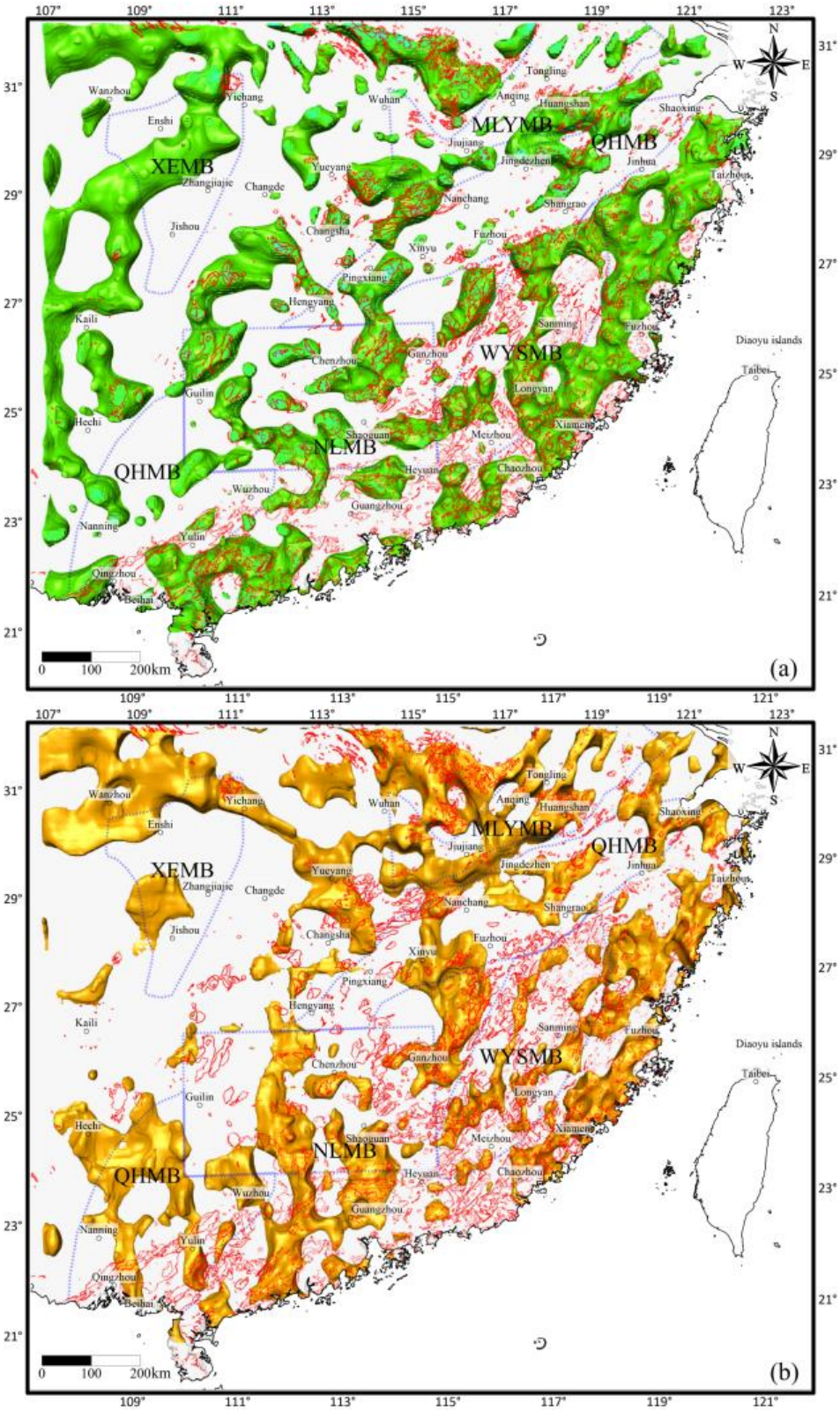

Figure 15. Birdview of low-density model (green isosurfaces) (a), high-susceptibility model (golden isosurfaces) (b) derived from gravity and magnetic inversion(as Figure12 show,depth is 30km), and outcrops of plutons (red lines) in South China

The Fe and Cu deposits in SC that are relevant to magmatic-hydrothermal fluid are closely related to slightly intermediate intrusions (Figure 16). For instance, the Fe and Cu deposits in MLYMB (dominated by Fe and Cu deposits) concentrate around high-susceptibility bodies, and the reasons are as follows. (i) Fe and Cu skarn deposits were formed owing to the interaction between intermediate magma and carbonatite strata; (ii) The Fe and Cu ores in MLYMB surrounded the intermediate-basic intrusions and formed deposits due to dioritic porphyrite magnetite in volcanic basins. The Cu deposits in the eastern segment of QHMB are more closely related to low-density bodies, while they are not obviously related to magnetic bodies. This is because most of the Cu deposits in QHMB are porphyritic and hydrothermal deposits associated with acidic intrusions, such as Dexing porphyry Cu deposit and Tongshan porphyry Cu deposit. Overall, the terminations of the mineral systems of magnetite in SC are closely related to the locations of intermediate-basic intrusions, while those of porphyry and hydrothermal Cu deposits in SC are related to acidic intrusions.

Most W and Sn deposits in SC are mainly distributed in NLMB and QHMB. As revealed in Figure 17, the W and Sn deposits are closely related to low-density bodies, and most notably, large deposits tend to be distributed in low-density areas. Meanwhile, they correspond to high-susceptibility bodies. All these indicate that the depositing position of the mineral systems of W and Sn deposits mostly occur around crust-derived remelted granites. For example, Zhuxi W deposit and Dahutang W deposit—the first and the second largest W deposits in the world respectively—are both located near low-density bodies.

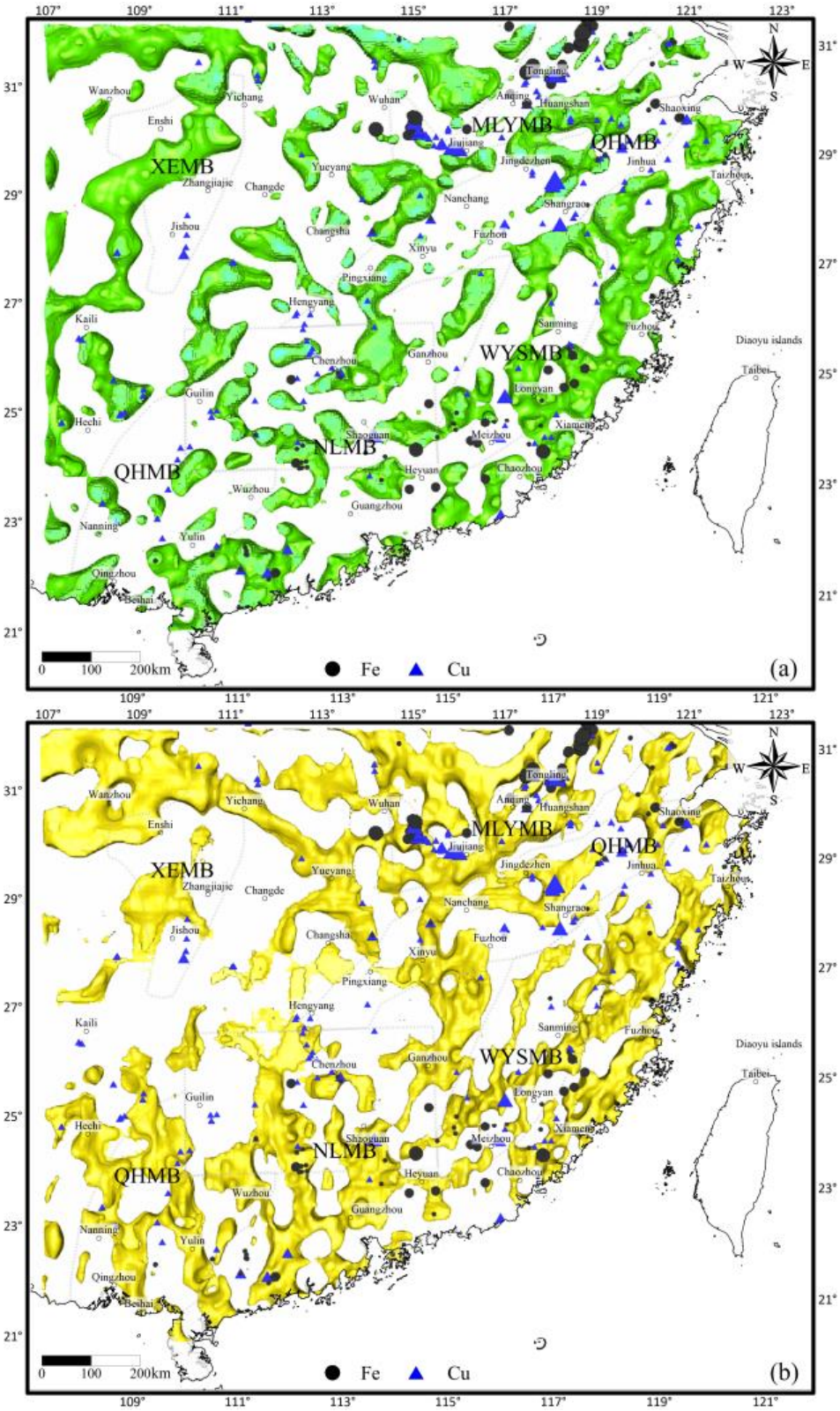

Figure 16.Birdview of low-density model (green isosurfaces) (a), high-susceptibility model (golden isosurfaces) (b) derived from gravity and magnetic inversion(as Figure12 show,depth is 30km), and locations of Fe and Cu deposits

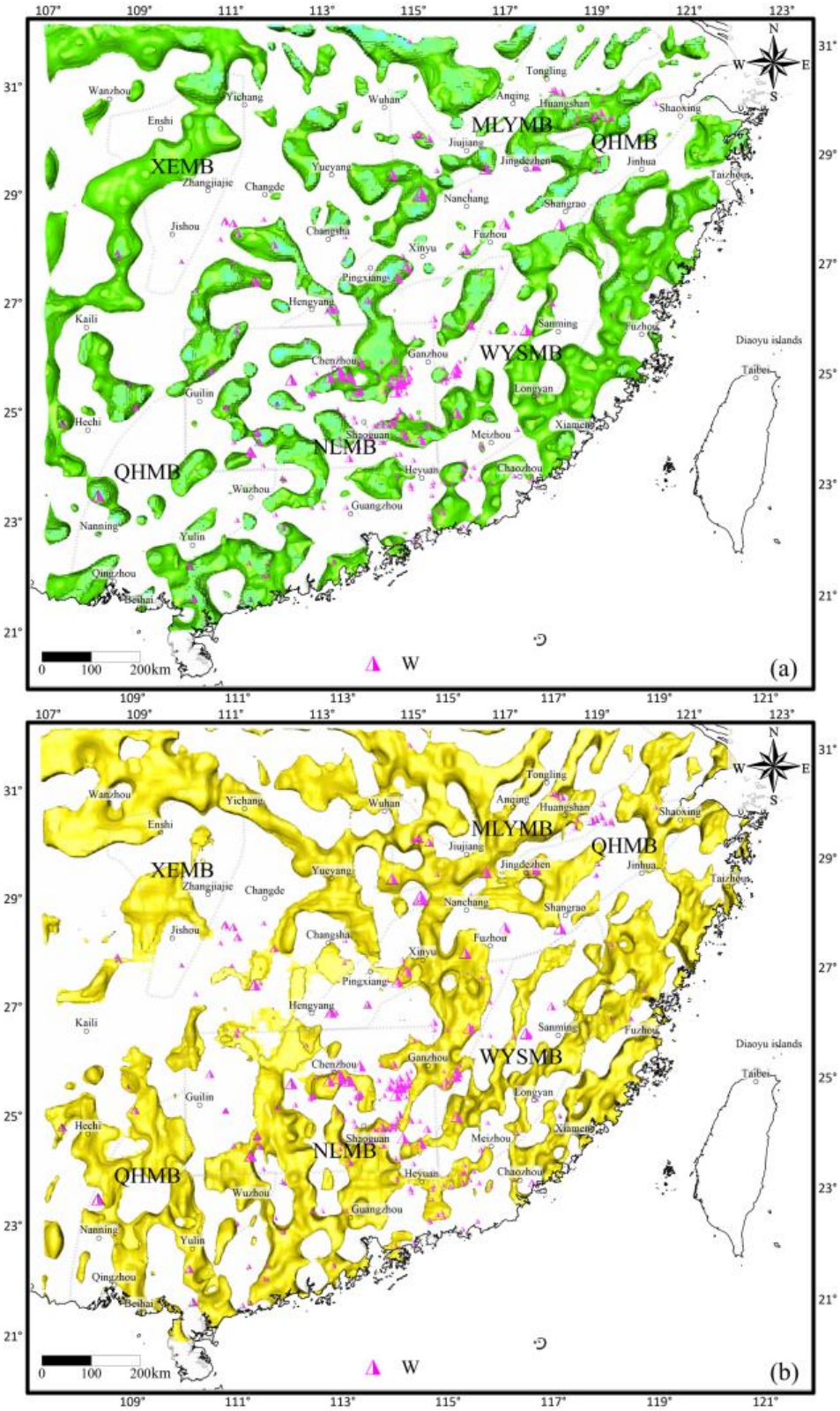

Figure 17. Birdview of low-density model (green isosurfaces) (a), high-susceptibility model (golden isosurfaces) (b) derived from gravity and magnetic inversion(as Figure12 show,depth is 30km), and locations of W and Sn deposits

5 Conclusions

(1) Vertical structures such as the Moho and magnetic basement in SC were obtained by processing and inversion of satellite gravity and magnetic data, the tectonic framework of SC was determined by multiscale edge detection of gravity and magnetic anomalies, and 3D density and magnetic structures were obtained through 3D gravity and magnetic inversion, thus providing deep information for research into the structure and mineralization of SC.

(2) The boundaries of JNO were redetermined. Its southern boundary is considered to be Shaoxin-Jinhua - Shangrao - north-Ganzhou – Chenzhou – Wuzhou - Yulin - east Beihai while its northern boundary is considered to be Huangshan - Jiujiang - Yueyang - Changde - Jishou– Kaili.

(3) The source zones of the mineral systems in major metallogenic belts in SC are reflected by the vertical structures of the lithosphere in this area. In MLYMB, the mineral systems of the Fe and Cu deposits have multi-level source zones. The initial-level source zone is the enriched mantle, which is formed owing to the thinning of the lithosphere and deformation caused by the fluids in the asthenosphere. In QHMB, the source zone of Cu deposits such as the Dexing deposit is the mantle, while the source zone of W deposits on the margin of the Moho uplift such as Zhuxi and Dahutang deposits is the remelted crust. As for QHMB, the W and Sn mineral systems originate from the crustal magma. In WYSMB, the diagenism and mineralization are mainly related to the interactions between materials in the crust and the mantle. The crust-derived materials form the deposits mainly containing W and rare earths, and mantle-derived materials form polymetallic deposits such as Cu and Au. As for XEMB, it consists mostly of metal deposits of the type of strata-bound sedimentation with the crust as the source zone, such as Sb, Pb, Zn, and Mn deposits.

(4) The pathways of the mineral systems of the major metallogenic belts in SC are deep faults and block or terrane boundaries determined by edge detection of gravity anomalies, as well as density contrast boundaries obtained with the 3D density model. The metallogenic pathways of Fe and Cu deposits in MLYMB mainly include the Yangtze River deep fault in NE trending and Tongling-Taizhou fault in SE trending and its secondary faults. The eastern segment of QHMB is mainly controlled by the faults in northeast Jiangxi, the southern segment of QHMB and the NLMB are

mainly under the control of the boundary faults of F1, and WYSMB is related to Zhenghe-Dapu fault and Heyuan-Shaowu fault.

(5) A 3D density and susceptibility model was obtained by 3D gravity and magnetic inversion. The distribution of different types of deposits was qualitatively reflected by different combination of density and susceptibility model, revealing the distribution of depositing position of different mineral systems in SC.

Acknowledgements

This study was jointly supported by the National Natural Science Foundation of China (Grant Nos.92062108,41630320,41574133) , China Geological Survey project (Grant Nos. DD20190012, DD20160082) and the National Key R&D Program of China (Grant No.2016YFC0600201).The earth gravity field Model EIGEN6C4 dataset download from GFZ(http://icgem.gfz-potsdam.de/home),EMAG2 dataset download from NOAA(https://www.ngdc.noaa.gov/geomag/emag2.html),we would like to express our heartfelt thanks to all of them.

Data Availability Statement

The gravity and magnetic data used in this paper can be accessed via repository: https://doi.org/10.6084/m9.figshare.13646771.

References

Andersen,O.B., Knudsen,P., Berry,P.A. M., 2010. The DNSC08GRA global marine gravity field fr om double retracked satellite altimetry. Journal of Geodesy , 84(3): 191-199.

Bolfan-Casanova, N., 2005. Water in the Earth's mantle. Mineralogical Magazine 69(3), 229-257.

Bott, M. H. P., 1960. The use of rapid digital computing methods for direct gravity interpretation of sedimentary basins. Geophysical Journal International 3(1), 63-67.

Andersen,O.B., Knudsen,P., Berry,P. M. 2010. The DNSC08GRA global marine gravity field from double retracked satellite altimetry. Journal of Geodesy , 84(3): 191-199.

Cawood, P.A., Wang, W., Zhao, T.Y., Xu, Y.J., Mulder, J.A., Pisarevsky, S.A., Zhang, L.M., Gan, C.S., He, H.Y., Liu, H.C., Qi, L., Wang, Y.J., Yao, J.L., Zhao, G.C., Zhou, M.F., Zi, J.W., 2020. Deconstructing South China and consequences for reconstructing Nuna and Rodinia. Earth-Science Reviews 204, 103169.

Charvet, J., 2013. The Neoproterozoic-Early Paleozoic tectonic evolution of the South China Block: An overview. Journal of Asian Earth Sciences 74, 198-209.

Chavez, R., Garland, G., 1985. Linear inversion of gravity data using the spectral expansion method. Geophysics 50(5), 820-824.

Chen, A.G., Lü, Q.T., Du, J.G., Yan, J.Y., 2019. The Poisson's ratio of the crust-mantle of South China and its geological significance. Geology in China 46(4), 750-758 (in Chinese with

English abstract).

Chen, J., Wang, R.C., Zhu, J.C., Lu, J.J., Ma, D.S., 2013. Multiple-aged granitoids and related tungsten-tin mineralization in the Nanling Range, South China. SCIENCE CHINA Earth Sciences 56, 2045.

Chen, Q., 2010. The evolution of Yunkai area and mineralization of precious metals. Sun YAT-SEN University(Natural Sciences Medicine) 31(04), 68-72 (in Chinese and English abstract).

Chen, Q., Sun, M., Zhao, G.C., Zhao, J.H., Zhu, W.L., Long, X.P., Wang, J., 2019. Episodic crustal growth and reworking of the Yudongzi terrane, South China: Constraints from the Archean TTGs and potassic granites and Paleoproterozoic amphibolites. Lithos 326-327, 1-18.

Chen, S.Zh, Ma, M., Chen, G., Zhou, Y., Zhu, X.T., Qiu, J.L., Mao, J.R., 2010. Taoxi Uplift of Wuyi Metallogenic Belt, Its Tectonics, Magmatism and Metallogeny. Earth Science—Journal of China University of Geosciences 35 (06), 969-984 (in Chinese with English abstract).

Chen, X.L., Liang, H.Y., Richards, J.P., Huang, W.T., Zhang, J., Wu, J., Sotiriou, P., 2018. Age and granite association of skarn W mineralization at Niutangjie district, South China Block. Ore Geology Reviews 102, 268-283.

Cheng, Z.Y., Yin, C.X., Zhu, J.L., 1985. Computing method for isostatic gravity anomalies. Geophysical & Geochemical exploration 9(5), 340-346 (in Chinese and English abstract).

Cordell, L., Henderson, R.G., 1968. Iterative three-dimensional solution of gravity anomaly data using a digital computer. Geophysics 33(4), 596-601.

Cormier, M.H., Macdonald, K.C., Wilson, D.S., 1995. A three-dimensional gravity analysis of the East Pacific Rise from 18° to 21° 30′ S. Journal of Geophysical Research: Solid Earth 100(B5), 8063-8082. https://doi.org/10.1029/95JB00243.

Deng, Y., Zhang, Z., Mooney, W., Badal, J., Fan, W., Zhong, Q., 2014. Mantle origin of the Emeishan large igneous province (South China) from the analysis of residual gravity anomalies. Lithos 204, 4-13. https://doi.org/10.1016/j.lithos.2014.02.008.

Ding, J.H., Fan, J.F., Ning, Y.J., Ling, L.Y., 2016. Geological charateristics and mineral resource potential of the Wuyishan Cu-Pb-Zn polymetallic metallogenic belt. Acta Geologica Sinica 90, 1537-1550 (in Chinese with English abstract).

Drummond, B.J., Goleby, B.R., Swager, C.P., Williams, P.R., 1993. Constraints on Archaean crustal composition and structure provided by deep seismic sounding in the Yilgarn Block. Ore Geology Reviews 8(1-2), 117-124.

Eyike,A., Werner,S. C., Ebbing, J.,Dicoum,E.M., 2010. On the use of global potential field models for regional interpretation of the West and Central African Rift System. Tectonophysics, 492(1-4): 25-39.

Feng, C.Y., Wang, H., Xiang, X.K., Zhang, M.Y., 2018. Late Mesozoic granite-related W-Sn mineralization in the northern Jiangxi region, SE China: A review. Journal of Geochemical Exploration 195, 31-48.

Feng, R., 1985. Crustal thickness and density in the upper mantle beneath china-the results of three dimensional gravity inversion. Acta Seismologica Sinica 7(2), 143-157 (in Chinese with English abstract).

Feng, R., Yan, H.F., Zhang, R.S., 1986a. The Rapia inversion of 3-D potential field and program design. Acta Geologica Sinica 4, 390-403 (in Chinese with English abstract).

Feng, R., 1986b. A computation method of potential field with three-dimensional density and magnetization distributions. Acta Geophysica Sinica 29(4), 309-406 (in Chinese with English abstract).

Feng, R., Wang, J., Zheng, S.Z., Yan, H.F., Zhou, H.N., Zhang, R.S., 1987. Isostaic status in North China (1)-Method and local compensation. Acta Seismologica Sinica 9(4), 406-416+443-444 (in Chinese with English abstract).

Greentree, M.R., Li, Z.X., 2008. The oldest known rocks in south-western China: SHRIMP U-Pb magmatic crystallisation age and detrital provenance analysis of the Paleoproterozoic Dahongshan Group. Journal of Asian Earth Sciences 33, 289-302.

Griffin, W.L., Begg, G.C., O'Reilly, S.Y., 2013. Continental-root control on the genesis of magmatic ore deposits. Nature Geoscience 6, 905-910.

Griffin, W.L., Begg, G.C., Suzanne, Y.O., 2013 Continental-root control on the genesis of magmatic ore deposits. Nature Geosci., 6: 905-910.

Grindlay, N.R., Madsen, J.A., Rommevaux-Jestin, C., Sclater, J., 1998. A different pattern of ridge segmentation and mantle Bouguer gravity anomalies along the ultra-slow spreading Southwest Indian Ridge (15° 30′ E to 25° E). Earth and Planetary Science Letters 161(1-4), 243-253. https://doi.org/10.1016/S0012-821X(98)00154-X.

Gu, X.X., Zhang, Y.M., Schulz, O., Vavtar, F., Liu, J.M., Zheng, M.H., Zheng, L., 2012. The Woxi W-Sb-Au deposit in Hunan, South China: An example of Late Proterozoic sedimentary exhalative (SEDEX) mineralization. Journal of Asian Earth Sciences 57, 54-75.

Guo, L., Gao, R., Meng, X., Zhang, G., 2015. A hybrid positive-and-negative curvature approach for detection of the edges of magnetic anomalies, and its application in the South China sea. Pure and Applied Geophysics 172(10), 2701-2710.

Guo, L., Shi, L., Meng, X., 2013. The antisymmetric factor method for magnetic reduction to the pole at low latitudes. Journal of Applied Geophysics, 92: 103-109.

Guo, L., Gao, R.,2018.Potential-field Evidence for the central and western Suture Zone Between the Yangtze and Cathaysia Blocks in South China. Precambrian Research,309：45-55.

Han, Q.S., Peng, S.B., Kusky, T., Polat, A., Jiang, X.F., Cen, Y., Liu, S.F., Deng, H., 2017. A Paleoproterozoic ophiolitic mélange, Yangtze craton, South China: Evidence for Paleoproterozoic suturing and microcontinent amalgamation. Precambrian Research 293, 13-38.

He, C., Dong, S., Santosh, M., Chen, X., 2013. Seismic evidence for a geosuture between the Yangtze and Cathaysia blocks, South China. Scientific reports 3, 2200.

Heinson, G., Didana, Y., Soeffky, P., Thiel, S., Wise, T., 2018. The crustal geophysical signature of a world-class magmatic mineral system. Scientific Reports 8, 1-6.

Heiskanen, W.A., 1967. Moritz H. Physical geodesy. Bulletin Geodesique 86(1), 491-492.

Hou, Z.Q., Li, Q., Gao, Y., Lu, Y., Yang, Z.S., Wang, R., Shen, Z., 2015. Lower-Crustal Magmatic Hornblendite in North China Craton: Insight into the Genesis of Porphyry Cu Deposits: Economic Geology, 110:1879-1904.

Hu, R.Z., Chen, W.T., Xu, D.R., Zhou, M.F., 2017. Reviews and new metallogenic models of mineral deposits in South China: An introduction. Journal of Asian Earth Sciences 137, 1-8.

Hu, R.Z., Wei, W.F., Bi, X.W., Peng, J.T., Qi, Y.Q., Wu, L.Y., Chen, Y.W., 2012. Molybdenite Re-Os and muscovite 40Ar/39Ar dating of the Xihuashan tungsten deposit, central Nanling district, South China. Lithos 150, 111-118.

Hu, R.Z., Zhou, M.F., 2012. Multiple Mesozoic mineralization events in South China—an introduction to the thematic issue. Mineralium Deposita 47, 579-588.

Hu, X.L., Gong, Y.J., Pi, D.H., Zhang, Z.J., Zeng, G.P., Xiong, S.F., Yao, S.Z., 2017. Jurassic magmatism related Pb-Zn-W-Mo polymetallic mineralization in the central Nanling Range, South China: Geochronologic, geochemical, and isotopic evidence from the Huangshaping

deposit. Ore Geology Reviews 91, 877-895.

Huang, L.C., Jiang, S.Y., 2014. Highly fractionated S-type granites from the giant Dahutang tungsten deposit in Jiangnan Orogen, Southeast China: geochronology, petrogenesis and their relationship with W-mineralization. Lithos 202-203, 207-226.

Huang, Z.L., Wang, D., Yan, J.-Y., Zhang H., 2016.A huge deep fault system at the east edge of Eurasia: the new tectonic interpretation based on satellite gravity. Acta Geoscientica Sinica,37(1):25-34.

Huston, D.L., Mernagh, T.P., Hagemann, S.G., Doublier, M.P., Fiorentini, M., Champion, D.C., Lynton Jaques, A., Czarnota, K., Cayley, R., Skirrow, R., Bastrakov, E., 2016. Tectono-metallogenic systems — The place of mineral systems within tectonic evolution, with an emphasis on Australian examples. Ore Geology Reviews 76, 168-210.

Ji, S.L. 2018. Metallogeny in Zhejiang Section of Wuyi Metallogenic Belt under Paleo-Pacific Plate Subduction Mechanism during the Late Mesozoic. Ph.D. thesie, Zhejiang University, China (in Chinese with English abstract).

Jiang, L., 2014. Research and implementation of terrain correction using sector cylinder models in spherical coordinate (Master's Thesis). Beijing: China University of Geosciences (Beijing),1-50.

Jiang, S.H., Bagas, L., Liang, Q.L., 2017. Pyrite Re-Os isotope systematics at the Zijinshan deposit of SW Fujian, China: Constraints on the timing and source of Cu-Au mineralization. Ore Geology Reviews 80, 612-622.

Laske, G., Masters, G., Ma, Z., Pasyanos, M., 2012. CRUST1. 0: An updated global model of Earth's crust. Geophys Res Abs 14, 3743.

Legros, H., Harlaux, M., Mercadier, J., Romer, R.L., Poujol, M., Camacho, A., Marignac, C., Cuney, M., Wang, R.C., Charles, N., Lespinasse, M.Y., 2020. The world-class Nanling metallogenic belt (Jiangxi, China): W and Sn deposition at 160 Ma followed by 30 m.y. of hydrothermal metal redistribution. Ore Geology Reviews 117, 103302.

Li, H., Kong, H., Zhou, Z.K., Tindell, T., Tang, Y.Q., Wu, Q.H., Xi, X.S., 2019. Genesis of the Banxi Sb deposit, South China: Constraints from wall-rock geochemistry, fluid inclusion microthermometry, Rb-Sr geochronology, and H-O-S isotopes. Ore Geology Reviews 115, 103162.

Li, H., Palinkaš, L.A., Watanabe, K., Xi, X.S., 2018. Petrogenesis of Jurassic A-type granites associated with Cu-Mo and W-Sn deposits in the central Nanling region, South China: Relation to mantle upwelling and intra-continental extension. Ore Geology Reviews 92, 449-462.

Li, K., Wu, C.X., Tang, C.Y., Duan, Q.F., Yu, Y.S., 2014. Carbon and oxygen isotopes of Pb-Zn ore deposits in western Hunan and eastern Guizhou provinces and their implications for the ore-forming process. Geology in China 41, 1608-1619 (in Chinese with English abstract).

Li, L.M., Lin, S.F., Davis, D.W., Xiao, W.J., Xing, G.F., Yin, C.Q., 2014. Geochronology and geochemistry of igneous rocks from the Kongling terrane: Implications for Mesoarchean to Paleoproterozoic crustal evolution of the Yangtze Block. Precambrian Research 255, 30-47.

Li, S.Z., Suo, Y.H., Li, X.Y., Zhou, J., Santosh, M., Wang, P.C., Wang, G.Z., Guo, L.L., Yu, S.Y., Lan, H.Y., Dai, L.M., Zhou, Z.Z., Cao, X.Z., Zhu, J.J., Liu, B., Jiang, S.H., Wang, G., Zhang, G.W., 2019. Mesozoic tectono-magmatic response in the East Asian ocean-continent connection zone to subduction of the Paleo-Pacific Plate. Earth-Science Reviews 192, 91-137.

Li, W.S., Ni, P., Wang, G.G., Yang, Y.L., Pan, J.Y., Wang, X.L., Chen, L.L., Fan, M.S., 2020. A possible linkage between highly fractionated granitoids and associated W-mineralization in the Mesozoic Yaogangxian granitic intrusion, Nanling region, South China. Journal of Asian

Earth Sciences 193, 104314.

Li, Y.G., Oldenburg, D.W., 1996. 3-D inversion of magnetic data. Geophysics 61(2), 394-408.

Li, Y.G., Oldenburg, D.W., 1998. 3-D inversion of gravity data. Geophyscis 63(1), 109-119.

Li, Y.H., Zheng, J.P., Ping, X.Q., Xiong, Q., Xiang, L., Zhang, H., 2018. Complex growth and reworking processes in the Yangtze cratonic nucleus. Precambrian Research 311, 262-277.

Liang, J, Zhou, Y.Zh., Li, H.Zh, Yin, Z.Z., Zhou, L.Y., Zeng, C.Y., Yu, P.P., 2012. Geological characteristics and genesis of porphyry copper deposits in Qinzhou-Hangzhou suture zone, South China. Acta Petrologica Sinica 28(10), 3361-3372 (in Chinese with English abstract).

Liang, J., Zhou, Y.Zh., Li, H.Zh., 2015. Tectonic evolution of the Juncture between Yangtze craton and Cathaysian block: Its significance for mineralization of porphyry copper deposits. Earth Science Frontiers 22(2), 144-159 (in Chinese with English abstract).

Liu G.D,2007.Geodynamical evolution and tectonic framework of China.Earth science frontiers.14(03):39-46.

Liu, B., Zhai, M.G., Zhao, L., Cui, X.H., Zhou, L.G., 2019. Zircon U-Pb-Hf isotope studies of the early Precambrian metasedimentary rocks in the Kongling terrane of the Yangtze Block, South China. Precambrian Research 320, 334-349.

Liu, L., 2015. Late Mesozoic Episodic Volcanism in SE China: Response to Paleo-Pacific Subduction. Ph.D. thesis, Nanjing University, China (in Chinese and English abstract).

Liu, Q., Yu, J.H., O'Reilly, S.Y., Zhou, M.F., Griffin, W.L., Wang, L.J., Cui, X., 2014. Origin and geological significance of Paleoproterozoic granites in the northeastern Cathaysia Block, South China. Precambrian Research 248, 72-95.

Liu, Y., Wang Q., Zhao J., 1978. A preliminary study based on gravity data of the crustal structure of the Peking-Tientsin area and its neighboring regions. ACTA GEOPHYSICA SINICA, 21(1), 9-17 (in Chinese with English abstract).

Liu, Y., Wang, Q., 1977. Inversion of gravity data by use of a method of "compressed mass plane" to estimate crustal structure. ACTA GEOPHYSICA SINICA 20(1), 61-71 (in Chinese with English abstract).

Long, Zh.L., 1999. Gravity isostatic anomalies and primary diamond deposits. Geophysical & Geochemical exploration, 23(3), 26-31+35 (in Chinese and English abstract).

Lü, Q.T., Meng, G.X., Yan, J.Y., Zhang, K., Gong, X.J., Gao, F.X., 2020. The geophysical exploration of Mesozoic iron-copper mineral system in the middle and lower reaches of Yangztez River metallogenic belt: A synthesis Earth Science Frontiers 27, DOI：10.13745/j.esf.sf.2020.3.18 (in Chinese with English abstract).

Lü, Q.T., Meng, G.X., Yan, J.Y., Zhang, K., Zhao, J.H., Gong, X.J., 2019. Multi-scale exploration of mineral system: Concept and progress-A case study in the middle and lowe reaches of the Yangtze River Metllogenic Belt. Geology in China 46, 673-689 (in Chinese with English abstract).

Lü, Q.T., Shi, D.N., Liu, Z.D., Zhang, Y.Q., Dong, S.W., Zhao, J.H., 2015. Crustal structure and geodynamics of the Middle and Lower reaches of Yangtze metallogenic belt and neighboring areas: Insights from deep seismic reflection profiling. Journal of Asian Earth Sciences 114, 704-716.

Luo, F., Yan, J.Y., Fu, G.M., Wang, H., Tao, X., Luo, L., 2019. Satellite gravity evidence of ore-forming material sources in metallogenic belts of South China. GEOLOGY IN CHINA 46(04), 759-774 (in Chinese with English abstract).

Luo, F.,Yan J.Y,Fu,G.M,Wang,H.,Tao,X.,Luo,L.,2019.Crust thickness and its apocalyptic of mineralization in South China: Constraint from Satellite Gravity data. Geology in China,

46(4): 759-774(in Chinese with English abstract).

Mao, J.W., Cheng, Y.B., Chen, M.H., Franco, P., 2013. Major types and time-space distribution of Mesozoic ore deposits in South China and their geodynamic settings. Mineralium Deposita 48, 267-294.

Mao, J.W., Xie, G.Q., Duan, C., Pirajno, F., Ishiyama, D., Chen, Y.C., 2011. A tectono-genetic model for porphyry-skarn-stratabound Cu-Au-Mo-Fe and magnetite-apatite deposits along the Middle-Lower Yangtze River Valley, Eastern China. Ore Geology Reviews 43, 294-314.

Mao, J.W., Xiong, B.K., Liu, J., Pirajno, F., Cheng, Y.B., Ye, H.S., Song, S.W., Dai, P., 2017. Molybdenite Re/Os dating, zircon U-Pb age and geochemistry of granitoids in the Yangchuling porphyry W-Mo deposit (Jiangnan tungsten ore belt), China: Implications for petrogenesis, mineralization and geodynamic setting. Lithos 286-287, 35-52.

Mao, J.W., Zhang, J.D., Pirajno, F., Ishiyama, D., Su, H.M., Guo, C.L., Chen, Y.C., 2011. Porphyry Cu-Au-Mo-epithermal Ag-Pb-Zn-distal hydrothermal Au deposits in the Dexing area, Jiangxi province, East China—A linked ore system. Ore Geology Reviews 43, 203-216.

Mao, W., Zhong, H., Zhu, W.G., Lin, X.G., Zhao, X.Y., 2018. Magmatic-hydrothermal evolution of the Yuanzhuding porphyry Cu-Mo deposit, South China: Insights from mica and quartz geochemistry. Ore Geology Reviews 101, 765-784.

Mao,J.,W., Li, X.F., Zhang, R. H., 2005. Deep fluid metallogenic system. Beijing.

Maus, S., Barckhausen, U., Berkenbosch, H., Bournas, N., Brozena, J., Childers, V., Dostaler, F., Fairhead, J., Finn, C., Vonfrese, R., 2009. EMAG2: A 2-arc min resolution earth magnetic anomaly grid compiled from satellite, airborne, and marine magnetic measurements. Geochemistry, Geophysics, Geosystems, 10(8):1-12.

McCuaig, TC, Beresford, S and Hronsky, J. 2010.Translating the mineral systems approach into an effective exploration targeting system: Ore Geology Reviews, 38:128–138.

McCuaig, TC and Hronsky, JMA.2014.The mineral system concept: The key to exploration targeting, in Building exploration capability for the 21st century edited by KD Kelley and HC Golden: Society of Economic Geologists, Inc, Special Publication 8:153–175.

Mooney, W.D., Kaban, M.K., 2010. The North American upper mantle: Density, composition, and evolution. Journal of Geophysical Research: Solid Earth 115(B12). https://doi.org/10.1029/2010JB000866.

Mungall, E.J., 2002. Roasting the mantle: Slab melting and the genesis of major Au and Au-rich Cu deposits. Geology, 30(10): 915.

Ni, P., Wang, G.G., 2017. Multiple episodes of Cu-Au mineralization in the northeastern section of the Qin-Hang metallogenic belt induced by reworking of continental crust. Acta Petrologica Sinica 33, 3373-3394 (in Chinese with English abstract).

Oldenburg, D., 1974. The inversion and interpretation of gravity anomalies. Geophysics 39(4), 526-536.

Pan, X.F., Hou, Z.Q., Li, Y., Chen, G.H., Zhao, M., Zhang, T.F., Zhang, C., Wei, J., Kang, C., 2017. Dating the giant Zhuxi W-Cu deposit (Taqian-Fuchun Ore Belt) in South China using molybdenite Re-Os and muscovite Ar-Ar system. Ore Geology Reviews 86, 719-733.

Parker, R., 1972. The rapid calculation of potential anomalies. Geophysical Journal of the Royal Astronomical Society 31, 447-455.

Parker, R.L., 1973. The rapid calculation of potential anomalies. Geophysical Journal International 31(4), 447-455. https://doi.org/10.1111/j.1365-246X.1973.tb06513.x.

Pavlis,N.K., Holmes, S.A., Kenyon, S.C., Factor, J. K., 2012. The development and evaluation

of the Earth Gravitational Model 2008 (EGM2008). Journal of Geophysical Research: Solid Earth [J], 117(B4).

Prince, R. A., Forsyth, D. W., 1988. Horizontal extent of anomalously thin crust near the Vema fracture zone from the three-dimensional analysis of gravity anomalies. Journal of Geophysical Research: Solid Earth 93(B7), 8051-8063. https://doi.org/10.1029/JB093iB07p08051.

Qi, Y.Q., Hu, R.Z., Gao, J.F., Leng, C.B., Gong, H., Gao, W., 2020. Late Mesozoic oxidized magma for porphyry Ag mineralization: A comparative study from mineralized and barren granite porphyries in the Lengshuikeng Ag-(Pb-Zn) deposit, South China. Journal of Asian Earth Sciences 190, 104180.

Qiu, X.F., Ling, W.L., Liu, X.M., Lu, S.S., Jiang, T., Wei, Y.X., Peng, L.H., Tan, J.J., 2018. Evolution of the Archean continental crust in the nucleus of the Yangtze block: Evidence from geochemistry of 3.0 Ga TTG gneisses in the Kongling high-grade metamorphic terrane, South China. Journal of Asian Earth Sciences 154, 149-161.

Radhakrishna, M., Lasitha, S., Mukhopadhyay, M., 2008. Seismicity, gravity anomalies and lithospheric structure of the Andaman arc, NE Indian Ocean. Tectonophysics 460(1-4), 248-262. https://doi.org/10.1016/j.tecto.2008.08.021.

Rudnick,R.L., 1995. Making continental crust. Nature, 387:571-578.

Schneider, M.E., Eggler, D.H., 1986. Fluids in equilibrium with peridotite minerals: implications for mantle metasomatism. Geochimica et Cosmochimica Acta 50(5), 711-724. https://doi.org/10.1016/0016-7037(86)90347-9.

Shi, D.N., Lü, Q.T., Xu, W.Y., Yan, J.Y., Zhao, J.H., Dong, S.W., Chang, Y.F., 2013. Crustal structure beneath the middle-lower Yangtze metallogenic belt in East China: Constraints from passive source seismic experiment on the Mesozoic intra-continental mineralizaiton. Tectonphysics 606, 48-60.

Shu, L.S., Faure, M., Yu, J.H., Jahn, B.M., 2011. Geochronological and geochemical features of the Cathaysia block (South China): New evidence for the Neoproterozoic breakup of Rodinia. Precambrian Research 187, 263-276.

Shu, X.J., Wang, X.L., Sun, T., Xu, X.S., Dai, M.N., 2011. Trace elements, U-Pb ages and Hf isotopes of zircons from Mesozoic granites in the western Nanling Range, South China: Implications for petrogenesis and W-Sn mineralization. Lithos 127, 468-482.

Spera, F.J., 1987. Dynamics of translithospheric migration of metasomatic fluid and alkaline magma. In Mantle metasomatism. Academic Press London 1-20.

Suo, Y., Li, S., Li, X., Guo, L., Wang, Y., 2016. Crustal thickness anomalies in the Indian Ocean inferred from gravity analysis. Geological Journal 51, 634-643. https://doi.org/10.1002/gj.2786.

Tang, S., Liu, T., 1999. Origin of the early Sinian Minle manganese deposit, Hunan Province, China. Ore Geology Reviews 15, 71-78.

Tang, Y.W., Xie, Y.L., Liu, L., Lan, T.G., Yang, J.L., Sebastien, M., Yin, R.C., Liang, S.S., Zhou, L.M., 2017. U-Pb, Re-Os and Ar-Ar dating of the Linghou polymetallic deposit, Southeastern China: Implications for metallogenesis of the Qingzhou-Hangzhou metallogenic belt. Journal of Asian Earth Sciences 137, 163-179.

Tomoda, Y., Aki, K., 1955. Use of the function (sinx)/x in gravity problems. Proceedings of the Japan Academy 31(7), 443-448.

Tsuboi, C., 1956. Crustal structure in northern and middle California from gravity-pendulum data. Geological Society of America Bulletin 67(12), 1641-1646.

Uieda, L., Barbosa, V.C., Braitenberg, C., 2016. Tesseroids: Forward-modeling gravitational fields

in spherical coordinates. Geophysics, 81(5): 41-48.

Wan, X.-Y., Zhang. R.-Y., Sui, X.-H., Chen, L., 2017. Analysis of earth field detection based on satellite data. Spacecraft engineering. 26(2): 121-129.

Wang, D.H., Chen, Y.C., Chen, Z.H., Liu, S.B., Xu, J.X., Zhang, J.J., Zeng, Z.L., Chen, F.W., Li, H.Q., Guo, C.L., 2007. Assessment on mineral resource in Nanling region and suggestion for further prospecting. Acta Geol. Sin. 81, 882-890 (in Chinese with English abstract).

Wang, D.H., Huang, F., Wang, Y., He, H.H., Li, X.M., Liu, X.X., Sheng, J.F., Liang, T., 2020. Regional metallogeny of Tungsten-tin-polymetallic deposits in Nanling region, South China. Ore Geology Reviews 120, 103305.

Wang, W., Zhou, M.F., 2014. Provenance and tectonic setting of the Paleo- to Mesoproterozoic Dongchuan Group in the southwestern Yangtze Block, South China: Implication for the breakup of the supercontinent Columbia. Tectonophysics 610, 110-127.

Wang, X., Ren, M.H., Chen, J., 2017. The muscovite granites: Parental rocks to the Nanling Range tungsten mineralization in South China. Ore Geology Reviews 88, 702-717.

Wang, X.C., Li, X.H., Li, Z.X., Li, Q.l., Tang, G.Q., Gao, Y.Y., Zhang, Q.R., Liu, Y., 2012. Episodic Precambrian crust growth: Evidence from U-Pb ages and Hf-O isotopes of zircon in the Nanhua Basin, central South China. Precambrian Research 222-223, 386-403.

Wang, Y.J., Zhang, Y.Z., Cawood, P.A., Zhou, Y.Z., Zhang, F.F., Yang, X., Cui, X., 2019. Early Neoproterozoic assembly and subsequent rifting in South China: Revealed from mafic and ultramafic rocks, central Jiangnan Orogen. Precambrian Research 331, 105367.

Wang, Z.W., Zhou, Y.Zh., 2002. Geological Characteristics and genesis of the pangxidong-Jinshan Ag-Au Deposit in Yunkai Terrain, South China. Geotectonic et Metallogenia 26(02), 193-198 (in Chinese and English abstract).

Williams, N.C., 2008. Geologically-constrained UBC-GIF gravity and magnetic inversions with examples from the Agnew-Wiluna greenstone belt, Western Australia. Ph.D. thesis, University of British Columbia, Canada.

Wu, C.Q., Zhang, Z.W., Xiao, J.F., Fu, Y.Z., Shao, S.X., Zheng, C.F., Yao, J.H., Xiao, C.Y., 2016. Nanhuan manganese deposits within restricted basins of the southeastern Yangtze Platform, China: Constraints from geological and geochemical evidence. Ore Geology Reviews 75, 76-99.

Wu, Y.B., Zheng, Y.F., 2013. Tectonic evolution of a composite collision orogen: An overview on the Qinling-Tongbai-Hong'an-Dabie-Sulu orogenic belt in central China. Gondwana Research 23, 1402-1428.

Wu, Y.B., Zheng, Y.F., Gao, S., Jiao, W.F., Liu, Y.S., 2008. Zircon U-Pb age and trace element evidence for Paleoproterozoic granulite-facies metamorphism and Archean crustal rocks in the Dabie Orogen. Lithos 101, 308-322.

Wyborn, L.A.I., Heinrich, C.A., Jaques, A.L., 1994. Australian Proterozoic mineral systems: essential ingredients and mappable criteria. AusIMM Publication Series 5, pp. 109-115.

Xia, Y., Xu, X.S., Niu, Y.L., Liu, L., 2018. Neoproterozoic amalgamation between Yangtze and Cathaysia blocks: The magmatism in various tectonic settings and continent-arc-continent collision. Precambrian Research 309, 56-87.

Xu, Y.H., Wang, C.Y., Zhao, T.P., 2016. Using detrital zircons from river sands to constrain major tectono-thermal events of the Cathaysia Block, SE China. Journal of Asian Earth Sciences 124, 1-13.

Yan, C.L., Shu, L.S., Michel, F., Chen, Y., Li, C., 2017. Early Paleozoic intracontinental orogeny in the Yunkai domain, South China Block: New insights from field observations, zircon U-Pb geochronological and geochemical investigations. Lithos 268-271, 320-333.

Yan, J.Y., Lü, Q.T., Chen, M.C., Deng, Z., Qi, G., Zhang, K., Liu, Z.D, Wang, J., Liu, Y., 2015. Identification and extraction of geological structure information based on multi-scale edge detection of gravity and magnetic fields: An example of the Tongling ore concentration area. Chinese J. Geophys 58(12), 4450-4464 (in Chinese with English abstract).

Yan, J.Y., Lü, Q.T., Luo, F., Chen, A.G., Ye, G.F., Zhang, Y.Q., Zhang, K., Zhao, J.H., Zhang, C., Liu, Z.D., Liu, Y., 2019. Where is Qinzhou-Hangzhou juncture belt? Evidence from integrated geophysical exploration. Geology in China 46(4), 690-703 (in Chinese with English abstract).

Yan, J.Y., Lü, Q.T., Meng, G.X., Zhao, J.H., Deng, Z., Liu, Y., 2011. Tectonic framework research of the Lower and Middle Yangtze metallogenic belt based on gravity and magnetic multi-scale edge detection. ACTA GEOLOGICA SINICA 85(5), 900-914 (in Chinese with English abstract).

Yang, M.G., Mei, Y.W., 1997. Characteistics of Geology and Metallization in the Qinzhou-Hangzhou paleoplate juncture. Geology and Mineral Resources of South China 3, 52-59 (in Chinese with English abstract).

Yang, X.Z., Xia, Q.K., Deloule, E., Dallai, L., Fan, Q.C., Feng, M., 2008. Water in minerals of the continental lithospheric mantle and overlying lower crust: a comparative study of peridotite and granulite xenoliths from the North China Craton. Chemical Geology 256(1-2), 33-45. https://doi.org/10.1016/j.chemgeo.2008.07.020.

Yang, Z.Y., Jiang, S.Y., 2019. Detrital zircons in metasedimentary rocks of Mayuan and Mamianshan Group from Cathaysia Block in northwestern Fujian Province, South China: New constraints on their formation ages and paleogeographic implication. Precambrian Research 320, 13-30.

Yao, J.L., Cawood, P.A., Shu, L.S., Zhao, G.C., 2019. Jiangnan Orogen, South China: A ~970-820 Ma Rodinia margin accretionary belt. Earth-Science Reviews 196, 102872.

Yin, C.Q., Lin, S.F., Davis, D.W., Zhao, G.C., Xiao, W.J., Li, L.M., He, Y.h., 2013. 2.1-1.85Ga tectonic events in the Yangtze Block, South China: Petrological and geochronological evidence from the Kongling Complex and implications for the reconstruction of supercontinent Columbia. Lithos 182-183, 200-210.

Yu, J.H., O'Reilly, S.Y., Wang, L.J., Griffin, W.L., Zhou, M.F., Zhang, M., Shu, L.S., 2010. Components and episodic growth of Precambrian crust in the Cathaysia Block, South China: Evidence from U-Pb ages and Hf isotopes of zircons in Neoproterozoic sediments. Precambrian Research 181, 97-114.

Yu, J.H., O'Reilly, S.Y., Zhou, M.F., Griffin, W.L., Wang, L.J., 2012. U-Pb geochronology and Hf-Nd isotopic geochemistry of the Badu Complex, Southeastern China: Implications for the Precambrian crustal evolution and paleogeography of the Cathaysia Block. Precambrian Research 222-223, 424-449.

Zhai, Y.S., 1999. On the Metallogenic System. Earth Science Frontiers 6, 13-27 (in Chinese with English abstract).

Zhai, Y.S., Xiong, Y.L., Yao, S.Z., Lin, X.D., 1996. Metallogeny of copper and iron deposits in the Eastern Yangtse Craton, east-central China. Ore Geology Reviews 11, 229-248.

Zhang, C.J., Fang, J., Ma, Z.J., 2003. Preliminary study on isostatic anomaly and recent tectonic stress field- Taking east sea and its eastern boundary seas as example. ACTA SEISMOLOGICA SINICA 25(1), 32-39 (in Chinese and English abstract).

Zhang, L., Yang, L.Q., Groves, D.I., Sun, S.C., Liu, Y., Wang, J.Y., Li, R.H., Wu, S.G., Gao, L., Guo, J.L., Chen, X.G., Chen, J.H., 2019. An overview of timing and structural geometry of gold, gold-antimony and antimony mineralization in the Jiangnan Orogen, southern China. Ore Geology Reviews 115, 103173.

Zhang, L.M., Zhang, Y.Z., Cui, X., Cawood, P.A., Wang, Y.J., Zhang, A.M., 2019. Mesoproterozoic rift setting of SW Hainan: Evidence from the gneissic granites and metasedimentary rocks. Precambrian Research 325, 69-87.

Zhang, S.H., Li, Z.X., Evans, D.A.D., Wu, H.C., Li, H.Y., Dong, J., 2012. Pre-Rodinia supercontinent Nuna shaping up: A global synthesis with new paleomagnetic results from North China. Earth and Planetary Science Letters 353-354, 145-155.

Zhang, X.S., Xu, X.S., Xia, Y., Liu, L., 2017. Early Paleozoic intracontinental orogeny and post-orogenic extension in the South China Block: Insights from volcanic rocks. Journal of Asian Earth Sciences 141, 24-42.

Zhang, Y., Zhang, S.X., Liang, Q., Chen, C., 2015. Application of boundary identifying technologies using gravity and magnetic maps in three-dimensional geological mapping of western Junggar area. Earth Science—Journal of China University of Geosciences 40(03), 431-440 (in Chinese with English abstract).

Zhang, Y.Q., Xu, Y., Shi, D.N., Yan, J.Y., Xu, Z.W., Zhao, J.H., 2019. Crustal thickness and attributes of the Qinhang metallogenic belt and its neighbors: A study based on broadband seismic receiver function. Geology in China 46(4), 723-736 (in Chinese with English abstract)

Zhao, G.C., 2015. Jiangnan Orogen in South China: Developing from divergent double subduction. Gondwana Research 27, 1173-1180.

Zhao, G.C., Cawood, P.A., 2012. Precambrian geology of China. Precambrian Research 222-223, 13-54.

Zhao, J.H., Li, Q.W., Liu, H., Wang, W., 2018. Neoproterozoic magmatism in the western and northern margins of the Yangtze Block (South China) controlled by slab subduction and subduction-transform-edge-propagator. Earth-Science Reviews 187, 1-18.

Zhao, W.W., Zhou, M.F., Li, Y.H.M., Zhao, Z., Gao, J.F., 2017. Genetic types, mineralization styles, and geodynamic settings of Mesozoic tungsten deposits in South China. Journal of Asian Earth Sciences 137, 109-140.

Zhao, X.F., Zhou, M.F., Li, J.W., Sun, M., Gao, J.F., Sun, W.H., Yang, J.H., 2010. Late Paleoproterozoic to early Mesoproterozoic Dongchuan Group in Yunnan, SW China: Implications for tectonic evolution of the Yangtze Block. Precambrian Research 182, 57-69.

Zheng, H., Wang, Y., Wang, H.-B., 2012., Simulation of geomagnetic aided submarine navigation based on EMAG2. Progress in Geophysics. 27(04): 1795-1803.

Zhou, T.F., Wang, S.W., Fan, Y., Yuan, F., Zhang, D.Y., White, N.C., 2015. A review of the intracontinental porphyry deposits in the Middle-Lower Yangtze River Valley metallogenic belt, Eastern China. Ore Geology Reviews 65, 433-456.

Zhou, X.M., 2003. Thoughts on the Study of Granite in South China. Geological Journal of China Universities 9(04), 556-565 (in Chinese).

Zhou, Y., Duan, Q.F, Tang, J.X., Cao, L., Li, F., Huang, H.L., Gan, J.M., 2014. The large-scale low-temperature mineralization of lead-zinc deposits in western Hunan: Evidence from fluid inclusions. Geology and Exploration 50(03), 515-532 .

Zhou, Y.Z., Li, X.Y., Zheng, Y., Sheng, W.J., He, J.G., Yu, P.P., Niu, J., Zeng, C.Y., 2017. Geological settings and metallogenesis of Qinzhou Bay-Hangzhou Bay orogenic juncture belt, South China. Acta Petrologica Sinica 33, 667-681 (in Chinese with English abstract).

Zhou, Z.B., Wen, H.J., Qin, C.J., Liu, L., 2017. Geochemical and isotopic evidence for a magmatic-hydrothermal origin of the polymetallic vein-type Zn-Pb deposits in the northwest margin of Jiangnan Orogen, South China. Ore Geology Reviews 86, 673-691.

Zhu, Y., Lai, S.C., Qin, J.F., Zhu, R.Z., Zhang, F.Y., Zhang, Z.Z., Zhao, S.W., 2019.

Neoproterozoic peraluminous granites in the western margin of the Yangtze Block, South China: Implications for the reworking of mature continental crust. Precambrian Research 333, 105443.